

# **Development of pH-responsive hydrogel films encapsulated with PEG-VEGF<sub>165</sub> bioconjugates for wound dressings**

Karuna Arya Malik

A Thesis

In the Department

Of

**Chemistry and Biochemistry**

Presented in Partial Fulfillment of the Requirements

For the Degree of

Master of Science (Chemistry) at

Concordia University

Montreal, Quebec, Canada

February 2025

© Karuna Arya Malik, 2025



## **Abstract**

### **Development of pH-responsive hydrogel films encapsulated with PEG-VEGF<sub>165</sub> bioconjugates for wound dressings applications**

**Karuna Arya Malik, M.Sc.**

Protein-based wound dressings have emerged as a topic of interest in chronic wound healing owing to their distinct physical, chemical, and biological characteristics. Growth factor proteins, such as platelet-derived growth factor and vascular endothelial growth factor (VEGF), play a pivotal role in wound healing by mediating angiogenic responses and promoting the formation of new blood vessels, thereby accelerating recovery. However, protein delivery faces several challenges that can be addressed through the bioconjugation of proteins with macromolecules, which enhances their stability, solubility, bioactivity, and half-life. Over the years, various chemical strategies have been developed to conjugate synthetic polymers onto proteins effectively. One such approach is the "grafting to" strategy, which involves the covalent attachment of pre-formed poly(ethylene glycol) (PEG) to target molecules like proteins or other macromolecules. This method improves the solubility, stability, and bioavailability of the target molecules.

Various formulations including foams, fibers, and hydrogel films have been explored for safe delivery of proteins and protein bioconjugates. Among these, polymeric hydrogel films have gained significant attention due to their non-cytotoxic nature, versatility, biocompatibility, and ability to provide a moist environment conducive to healing.

My MSc research project focuses on developing hydrogel films crosslinked with boronic ester bonds that encapsulate PEG-VEGF<sub>165</sub> bioconjugates to promote the healing process in chronic wounds. The bioconjugates were characterized using techniques such as gel electrophoresis and dynamic light scattering. Additionally, hydrogel films were fabricated with biocompatible poly(vinyl alcohol) (PVA) crosslinked with tetrahydroxydiboronic (THDB), a diboronic acid crosslinker, ensuring dimensional stability and effective encapsulation of the bioconjugates. These hydrogels degraded in response to acidic and alkali pHs, hydrogen peroxide, and glucose, which could be found in wounds, leading to enhanced release of encapsulated PEG-VEGF bioconjugates.

These results, combined with antimicrobial properties, suggest that the developed THDB-PVA/bioconjugate crosslinked films possess great potential for designing dermal wound healing systems.

## Acknowledgements

First and foremost, I would like to express my heartfelt gratitude to my research supervisor, Dr. John Oh, for his invaluable guidance, continuous support, and encouragement throughout my Master's journey. I deeply appreciate the time and effort he dedicated to mentoring me, and I am truly grateful for the opportunity to learn under his supervision. I sincerely thank my amazing committee members, Dr. Rafik Naccache and Dr. Xia Li for their insightful suggestions and incredibly motivating feedback during my committee advisory meetings.

My appreciation extends to Prof. Judith Kornblatt, Dr. Chris Law, Dr. Anne Noronha, Dr. Brandon Findlay, and Farhan Rahman Chowdhury at Concordia as well as Prof. Marc-André Fortin and Zongyi Liu at Laval University for their helps and supports for my research. I would like to thank Sofia and Kadmbari for their technical help and fruitful discussions as well as all the members of Oh research group for their support. I had countless great memories with the members during my time at Concordia University.

I thank funding agencies for financial support to my MSc research, including NSERC discovery grant, Canada Research Chair, and NSERC CREATE entitled Polymer Nanoparticles for Drug Delivery (POND) program as well as Le Fonds de recherche du Québec – Nature et Technologies (FRQNT) Team Grant. I also thank Concordia University for various scholarships and fellowships, which include Poole chemistry Grad scholarship, Garnet strong scholarship, Split merit scholarship, Kanfi holzbaur award.

And last but definitely not least, I am indebted to my family, my amazing parents Sukhbir, Mukesh and my wonderful sisters and brothers for all their love and sacrifices that made it possible for me to pursue my dream of being a scientist. I would also like to extend my heartfelt thanks to my extended family for their encouragement and love, which have been a significant part of my journey. I am truly fortunate to have such a supportive and inspiring family. And finally, words cannot express how grateful I am to my boyfriend, Saaru, for his endless support, constant encouragement and for always being my guiding light and ray of sunshine.

## **Contribution of Authors**

All research described in this thesis was conducted independently under the supervision of Dr. John Oh at Concordia University. Most of experiments and data analysis were conducted by me, except for following experiments, including the synthesis of PEG-CI precursor by Kadambari Kadambari (PhD student in Dr. Oh's lab) as well as the synthesis of PEG-VS precursor, experimental design for bioconjugation, analysis of gel electrophoresis, and anti-microbial studies by Sofia Nieves Casillas Popova (PhD student in Dr. Oh's lab). Fluorescence microscopy by Dr. Chris Law in the Center of Microscopy (Biology) and CD experiments under the guidance of Dr. Anne Noronha (Chemistry and Biochemistry) were conducted.

# Table of Contents

|   |           |
|---|-----------|
| List of Figures.....  | xi        |
| List of Tables.....   | xiii      |
| List of Abbreviations.....  | xiv       |
| <br>  |           |
| <b>Chapter 1.....</b>   | <b>1</b>  |
| <b>Introduction.....</b>  | <b>1</b>  |
| <b>1.1 Overview of the research.....</b>                                | <b>1</b>  |
| <b>1.2 Wound dressings.....</b>   | <b>1</b>  |
| <b>1.3 Proteins in wound healing.....</b>                               | <b>4</b>  |
| 1.3.1 Subcategories of proteins in wound healing.....                   | 4         |
| 1.3.2 Vascular endothelial growth factor (VEGF) .....                   | 5         |
| <b>1.4 Challenges in direct delivery of proteins.....</b>               | <b>6</b>  |
| 1.4.1 Physical encapsulation.....                                       | 6         |
| 1.4.2 Bioaffinity GF immobilization.....                                | 7         |
| 1.4.3 Covalent attachment.....  | 8         |
| <b>1.5 Approaches to synthesize polymer-protein bioconjugates.....</b>  | <b>9</b>  |
| 1.5.1 Grafting to.....  | 9         |
| 1.5.2 Grafting from.....  | 9         |
| 1.5.3 Grafting through.....   | 9         |
| <b>1.6 PEGylation of proteins.....</b>                                  | <b>10</b> |
| <b>1.7 Type of delivery vehicles in wound healing applications.....</b> | <b>11</b> |
| 1.7.1 Foam and spongy scaffolds.....                                    | 12        |
| 1.7.2 Nanofibrous matrices.....   | 14        |
| 1.7.3 Hydrogels.....  | 15        |
| <b>1.8 PVA-based and boronic ester-crosslinked hydrogels.....</b>       | <b>18</b> |
| 1.8.1 PVA-based hydrogels.....  | 18        |

|  |           |
|--|-----------|
| 1.8.2 Boronic ester-crosslinked hydrogels.....   | 19        |
| <b>1.9 Scope of the thesis.....</b>  | <b>22</b> |
| <b>Chapter 2.....</b>  | <b>24</b> |
| <b>Experimental and Methods.....</b>   | <b>24</b> |
| <b>2.1 Experimental.....</b>   | <b>24</b> |
| 2.1.1 Instrumentation.....   | 24        |
| 2.1.2 Materials.....   | 24        |
| 2.1.3 Synthesis of PEG-VEGF <sub>165</sub> bioconjugates using CDI-mediated coupling reaction..... | 25        |
| 2.1.3.1 Synthesis of PEG-CI.....   | 25        |
| 2.1.3.2 Model reaction of PEG-CI with DEG-DSH.....   | 25        |
| 2.1.3.3 Bioconjugation of PEG-CI with VEGF <sub>165</sub> .....                                    | 26        |
| 2.1.4 Synthesis of PEG-VEGF <sub>165</sub> bioconjugates using DVS-mediated coupling reaction..... | 26        |
| 2.1.4.1 Synthesis of PEG-VS.....   | 26        |
| 2.1.4.2 Bioconjugation of PEG-VS with VEGF <sub>165</sub> .....                                    | 26        |
| 2.1.5 Gel electrophoresis.....   | 26        |
| 2.1.6 Fabrication of BE-crosslinked PVA hydrogels.....   | 27        |
| 2.1.6.1 General procedure for <i>in-situ</i> crosslinking approach.....                            | 27        |
| 2.1.6.2 General procedure for post-crosslinking approach.....                                      | 28        |
| 2.1.6.3 Gel content and swelling ratio.....  | 28        |
| 2.1.7 Stimuli-responsive degradation of THDB-PVA films.....  | 28        |
| 2.1.8 Encapsulation of PEG-VEGF <sub>165</sub> bioconjugates in THDB- PVA films.....               | 29        |
| 2.1.9 pH-responsive release of PEG-VEGF <sub>165</sub> bioconjugates using Bradford Assay.....     | 29        |
| 2.1.10 Fluorescence microscopy to locate bioconjugates in THDB-PVA/bioconjugate films.....         | 29        |

|  |               |
|--|---------------|
| 2.1.11 Fabrication of LF-loaded THDB-PVA/PEG-VEGF films.....   | 30            |
| 2.1.12 Antimicrobial test with disk diffusion method.....  | 30            |
| <b>2.2 Methodologies and principles.....</b>   | <b>30</b>     |
| 2.2.1 SDS-PAGE gel electrophoresis.....  | 30            |
| 2.2.2 Dynamic light scattering (DLS) .....   | 32            |
| 2.2.3 Circular Dichroism (CD) spectroscopy.....  | 32            |
| 2.2.4 FT-IR spectroscopy.....  | 33            |
| 2.2.5 Disc diffusion method to test antimicrobial properties.....  | 33            |
| <br><b>Chapter 3.....</b>  | <br><b>35</b> |
| <b>Result and Discussion.....</b>  | <b>35</b>     |
| <b>3.1 PEGylation of VEGF<sub>165</sub> protein to synthesize PEG-VEGF<sub>165</sub> bioconjugates.....</b>    | <b>35</b>     |
| 3.1.1 Approach I exploring CDI-mediated coupling reaction.....   | 35            |
| 3.1.2 Approach II exploring DVS-mediated coupling reaction.....  | 40            |
| <b>3.2 Fabrication of BE-crosslinked PVA hydrogels.....</b>  | <b>42</b>     |
| 3.2.1 In-situ crosslinking approach.....   | 42            |
| 3.2.2 Post-crosslinking approach.....  | 45            |
| <b>3.3 Studies of stimuli-responsive degradation (SRD) of THDB-PVA films.....</b>                              | <b>48</b>     |
| <b>3.4 Encapsulation and location analysis of PEG-VEGF<sub>165</sub> bioconjugates in THDB-PVA films.....</b>  | <b>50</b>     |
| <b>3.5 pH responsive release of PEG-VEGF<sub>165</sub> bioconjugates from THDB-PVA/bioconjugate films.....</b> | <b>52</b>     |
| <b>3.6 Fabrication and antimicrobial properties of LF/THDB-PVA/bioconjugate film.....</b>                      | <b>54</b>     |
| <b>3.7 Supplementary Figures for Chapter 3 .....</b>   | <b>55</b>     |
| <br><b>Chapter 4.....</b>  | <br><b>57</b> |

|   |           |
|---|-----------|
| <b>Conclusion and Future Work .....</b> | <b>57</b> |
| <b>4.1 Conclusion.....</b>              | <b>57</b> |
| <b>4.2 Future work.....</b>             | <b>58</b> |
| <b>References .....</b>                 | <b>59</b> |

## List of Figures

|  |    |
|--|----|
| <b>Figure 1.1</b> Schematic representation of four distinct stages in wound healing.....   | 2  |
| <b>Figure 1.2</b> Schematic representation of limitations in direct delivery of growth factors.....  | 6  |
| <b>Figure 1.3</b> Schematic illustration for delivery of GF's, including (a) physical encapsulation, (b) bioaffinity, and (c) covalent attachment.....                                       | 8  |
| <b>Figure 1.4</b> Schematic illustration of three distinct approaches to synthesize polymer-protein bioconjugates.....   | 10 |
| <b>Figure 1.5</b> Schematic illustration of specific sites in proteins for covalent attachment.....  | 11 |
| <b>Figure 1.6</b> Schematic illustration of an ideal wound dressing.....   | 12 |
| <b>Figure 1.7</b> Typical characteristic features of a hydrogel.....   | 16 |
| <b>Figure 1.8</b> Typical diboronic and boric acid crosslinkers reported in literature.....  | 19 |
| <b>Figure 1.9</b> Schematic representation to synthesize glucose-responsive hydrogels crosslinked using bisboronic acid and release of encapsulated insulin under SRD conditions.....        | 20 |
| <b>Figure 1.10</b> Schematic illustration to fabricate polymeric hydrogels from a mixture of a branched catechol-derivatized poly(ethylene glycol) with BDBA diboronic acid crosslinker..... | 21 |
| <b>Figure 1.11</b> Schematic demonstration of Chitosan/PVA/TAF <sub>e</sub> hydrogel crosslinked with phenylboronic acid.....  | 22 |
| <b>Figure 2.1</b> Sequence and amino acid composition in VEGF <sub>165</sub> .....   | 25 |
| <b>Figure 2.2</b> Digital image to show a setup to prepare gels.....   | 27 |
| <b>Figure 2.3</b> Digital image of a setup for gel electrophoresis.....  | 31 |
| <b>Figure 2.4</b> Schematic illustration of Kirby Bauer disc diffusion method for antibiotic susceptibility testing.....   | 34 |
| <b>Figure 3.1</b> Schematic illustration of approach I exploring CDI-mediated coupling reaction to synthesize well-defined PEG-VEGF <sub>165</sub> bioconjugate.....                         | 35 |
| <b>Figure 3.2</b> <sup>1</sup> H NMR spectrum of PEG-CI in CDCl <sub>3</sub> .....   | 36 |
| <b>Figure 3.3</b> a) Synthetic scheme of model reaction of PEG-CI with DEG-DSH and b) <sup>1</sup> H NMR spectrum of PEG-DEG-DS-PEG in CDCl <sub>3</sub> .....                               | 37 |
| <b>Figure 3.4</b> Evaluation of PEG-VEGF <sub>165</sub> bioconjugates prepared at PEG/VEGF <sub>165</sub> = 50/1, 100/1, 200/1, 300/1 wt/wt by native SDS-PAGE gel electrophoresis.....      | 38 |

|   |    |
|---|----|
| <b>Figure 3.5</b> DLS diagrams of (a) PEG-CI and (b) PEGCI-VEGF <sub>165</sub> bioconjugate prepared via Approach I.....  | 39 |
| <b>Figure 3.6</b> CD spectra of PEG-VEGF <sub>165</sub> bioconjugate (red) prepared using Approach I and bare VEGF <sub>165</sub> protein (purple) for comparison.....                                | 40 |
| <b>Figure 3.7</b> Schematic illustration of approach II exploring DVS-mediated coupling reaction to synthesize well-defined PEG-VEGF <sub>165</sub> bioconjugate.....                                 | 40 |
| <b>Figure 3.8</b> <sup>1</sup> H NMR spectrum of PEG-VS in CDCl <sub>3</sub> .....  | 41 |
| <b>Figure 3.9</b> DLS diagrams of (a) PEG-VS and (b) PEG-VEGF <sub>165</sub> bioconjugate prepared using approach II.....   | 42 |
| <b>Figure 3.10</b> Schematic illustration of in-situ crosslinking approach.....   | 42 |
| <b>Figure 3.11</b> Chemical structure of diboronic acid crosslinkers including BDB, BA and THDB.....  | 43 |
| <b>Figure 3.12</b> (a) Schematic illustration of post crosslinking approach and (b) crosslinking mechanism by the reaction of PVA with THBD to yield THDB-PVA hydrogel films.....                     | 46 |
| <b>Figure 3.13</b> FT-IR spectra of PC-1, 2 and 3 hydrogels films, compared with uncrosslinked PVA as a control.....  | 48 |
| <b>Figure 3.14</b> %Degradation of THDB-PVA films in response to (a) pHs, (b) zoomed in version pH's (c) glucose, and (d) hydrogen peroxide.....  | 49 |
| <b>Figure 3.15</b> Schematic illustration for the encapsulation of PEG-VEGF <sub>165</sub> bioconjugates in THDB-PVA film to fabricate THDB-PVA/bioconjugate films.....                               | 50 |
| <b>Figure 3.16</b> Scheme illustration of the reaction of fluorescamine with amine groups in proteins to form fluorescent products for fluorescence microscopy.....                                   | 51 |
| <b>Figure 3.17</b> (a) THDB-PVA film encapsulated with VEGF <sub>165</sub> , (b) THDB-PVA/bioconjugate film with (b) and without (c) VEGF <sub>165</sub> as a negative control.....                   | 52 |
| <b>Figure 3.18</b> Correlation curve of absorbance at 595 nm over concentration of BSA, a model protein in aqueous solution containing Coomassie dye.....   | 53 |
| <b>Figure 3.19</b> %Release of PEG-VEGF <sub>165</sub> bioconjugates from THDB-PVA/bioconjugate films incubated at different pHs. ....  | 53 |
| <b>Figure 3.20</b> a) DOI and b) digital images of LF itself, crosslinked and uncrosslinked LF/THDB-PVA/bioconjugate films over Gram-negative <i>E. coli</i> and Gram-positive <i>S. aureus</i> ..... | 55 |
| <b>Figure S3.1</b> CD spectra of BSA model protein.....   | 55 |
| <b>Figure S3.2</b> Overlaid UV-vis spectra of aqueous solutions of various concentrations up to 13 µg/mL containing Bradford reagent.....   | 56 |
| <b>Fig S3.3</b> Overlaid UV-Vis spectrums illustrating the % release of bioconjugates from incubated pieces of THDB-PVA/bioconjugate films at different pH values (5.4, 7.4, and 8.4) .....           | 56 |

## List of Tables

|  |    |
|--|----|
| <b>Table 3.1</b> Characteristics, appearance, and digital images of wet BE-crosslinked PVA hydrogels with water, prepared with diboronic acid crosslinkers including BDB, THDB and boric acid..... | 43 |
| <b>Table 3.2</b> Characteristics, properties, and digital images of THDB-PVA hydrogels.....  | 44 |
| <b>Table 3.3</b> Characteristics and digital images of THDB-PVA hydrogels prepared with aqueous THBD crosslinker solution.....   | 45 |
| <b>Table 3.4</b> Characteristics, properties, and digital images of THDB-PVA hydrogel films prepared by post crosslinking approach. ....   | 47 |

## List of Abbreviations

|                               |   |
|-------------------------------|---|
| APS                           | Ammonium persulfate                     |
| ATRP                          | Atom Transfer Radical Polymerization    |
| BA                            | Boronic acid                            |
| BE                            | Boronic ester                           |
| BSA                           | Bovine serum albumin                    |
| bFGF                          | Basic fibroblast growth factor          |
| BMP-2                         | Bone morphogenetic protein-2            |
| BPDBA                         | 4,4'-biphenyldiboronic acid             |
| BDBA                          | Benzene-1,4-diboronic acid              |
| CD                            | Circular dichroism spectroscopy         |
| CDI                           | Carbonyl diimidazole                    |
| CRP                           | Controlled radical polymerization       |
| Cys                           | Cysteine                                |
| DCM                           | Dichloromethane                         |
| DOI                           | Diameter of inhibition                  |
| DBU                           | 1,8-diazabicyclo[5.4.0]undec-7-ene      |
| DEG-DSH                       | 2,2'-(ethylenedioxy)diethanethiol       |
| DLS                           | Dynamic light scattering                |
| DMSO                          | Dimethyl sulfoxide                      |
| DVS                           | Divinyl sulfone                         |
| EGF                           | Epidermal growth factor                 |
| ECM                           | Extra cellular matrix                   |
| FDA                           | Food and Drug Administration            |
| FT-IR                         | Fourier transform infrared spectroscopy |
| GelMA                         | Gelatin methacryloyl                    |
| Glu                           | Glutamine                               |
| GF                            | Growth Factor                           |
| H <sub>2</sub> O <sub>2</sub> | Hydrogen peroxide                       |

|                |  |
|----------------|--|
| HCl            | Hydrochloric Acid                                      |
| HPC            | Hydroxypropylcellulose                                 |
| LF             | Levofloxacin   |
| Lys            | Lysine   |
| MHB            | Muller Hinton broth 2                                  |
| NaH            | Sodium hydride   |
| NaOH           | Sodium hydroxide                                       |
| PBS            | Phosphate buffered saline                              |
| PCL            | Poly( $\epsilon$ -caprolactone)                        |
| PLA            | Poly(lactic acid)                                      |
| PLACL          | Poly(L-lactic acid)-co-poly( $\epsilon$ -caprolactone) |
| PLGA           | Poly(L-lactic acid-co-glycolic acid)                   |
| PLLA           | Poly(L-lactic acid)                                    |
| PVA            | Poly(vinyl alcohol)                                    |
| PU             | Polyurethane   |
| rhEGF          | Recombinant human epidermal growth factor              |
| RAFT           | Reversible Addition-Fragmentation Chain Transfer       |
| ROS            | Reactive oxygen species                                |
| SDS            | Sodium dodecyl sulfate                                 |
| SDS-PAGE       | Sodium dodecyl sulphate polyacrylamide                 |
| SRD            | Stimuli responsive degradation                         |
| TGF- $\beta$ 1 | Transforming growth factor-beta                        |
| TEMED          | Tetramethyl ethylenediamine                            |
| THB            | Tetrahydroxyborate                                     |
| THDB           | Tetrahydroxydiboronic acid                             |
| UV             | Ultraviolet  |
| UV/vis         | Ultraviolet spectroscopy                               |
| VIP            | Vasoactive intestinal peptide                          |
| VEGF           | Vascular endothelial growth factor                     |

# Introduction

## 1.1 Overview of the research

My MSc research aims at the development of PVA-based hydrogel films crosslinked with boronic ester bonds that are encapsulated with PEG-VEGF<sub>165</sub> bioconjugates to promote healing process in chronic wounds. This research began with PEGylation of VEGF through well-known click-type reactions named as carbodiimide (CDI)-mediated and divinylbenzene (DVS)-mediated conjugation reactions. Systematic investigation allows for the fabrication dimensionally stable PVA hydrogel films crosslinked with boronic ester bonds through the use of THDB diboronic acid crosslinker. These hydrogel films degraded in response to stimuli such as acidic and alkali pHs, hydrogen peroxide (as typical reactive oxygen species), and glucose, all of which could be found in wounds. Given the optimized protocol, the synthesized PEG-VEGF bioconjugates were encapsulated in the hydrogels and their locations in hydrogels were studied using fluorescence microscopy. They were further explored for pH-responsive release of bioconjugates using Bradford-protein assay. For our preliminary investigation to demonstrate the potential of PVA hydrogel films for wound dressing, they were evaluated for antimicrobial properties following the incorporation of levofloxacin.

## 1.2 Wound dressings

Wound healing is a dynamic and complicated process, which needs an appropriate environment to promote accelerated healing. A wound occurs when skin's epithelial or mucosal lining disintegrates due to a physical or thermal injury<sup>1</sup>. Wounds are classified as acute or chronic based on their nature and healing time<sup>2,3</sup>. An acute wound is a sudden damage to the skin from an accident or surgery and typically recovers within 8-12 weeks, depending on the size, depth, and amount of damage in the epidermis and dermis layers<sup>4</sup>. Chronic wound shows inadequate healing, delayed repair and generally results from decubitus ulcer, leg ulcer and burns<sup>5</sup>. It has been reported that the key reason for the difference in both types of wounds is prolonged healing time in chronic wounds<sup>6</sup>. As illustrated in Figure 1.1, wound healing involves four distinct stages of tissue regeneration and growth, including: (A) coagulation and haemostasis phase (immediately after injury), (B) inflammatory phase (swelling), (C) proliferation period (formation of new tissues and

blood vessels), and (D) maturation phase (remodeling of new tissues)<sup>7, 8</sup>. Acute wounds often heal in an organized and efficient way, progressing smoothly through all four stages of wound healing. In contrast, chronic wounds similarly begin the healing process, but have prolonged inflammatory, proliferative, or remodeling phases. This imbalance often results in a chronic state of inflammation, delayed tissue regeneration, and excessive scarring. Over time, these disruptions can cause tissue fibrosis and the formation of non-healing ulcers, which significantly increase the risk of complications and pose challenges for effective treatment<sup>6</sup>.

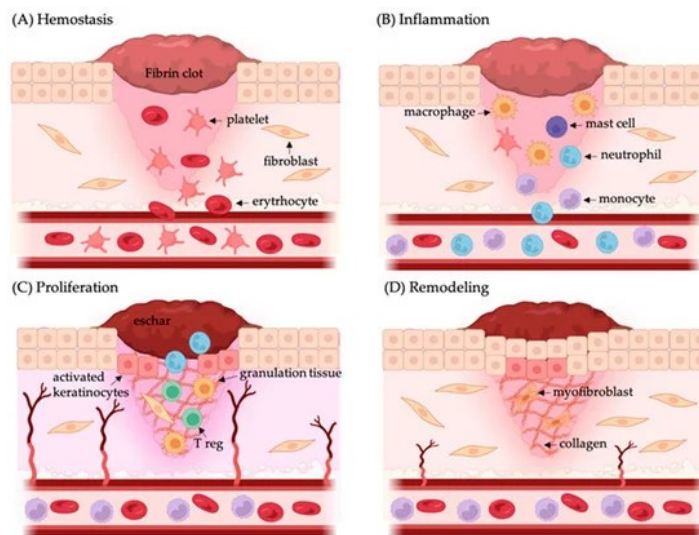


**Figure 1.1** Schematic representation of four distinct stages in wound healing<sup>9</sup>. Copyright 2024, MDPI.

Wound care has been developed for a long time, for example, in 2500 BC, Mesopotamians treated wounds with clay tablets. They cleaned the wounds with milk or water before applying the resin and honey. Hippocrates of ancient Greece utilized wine or vinegar to clean wounds between 460-370 BC. They used wool boiled in water or wine as a bandage<sup>10</sup>. Until the mid-1900s, it was widely believed that wounds heal faster when left dry and uncovered. However, an Egyptian medical literature, Edwin Smith's surgical papyrus from 1615 BC, states that closed wounds heal faster than open ones because closed wounds are exposed to proteinases, chemotactic, complement, and growth factors, which is lost in the wound exposed<sup>11</sup>.

Traditional wound dressings were primarily aimed to shield the wound from direct contamination by bacteria. For instance, gauze dressings developed using cotton, rayon, and polyester fibers offer some protection against bacterial infections. Sterile gauze pads with fibers can absorb exudates and fluid from open wounds. These dressings require frequent changing to prevent maceration of healthy tissues. Excessive wound drainage causes bandages to become moist and stick to the site, causing pain when removed. Therefore, traditional dressings failed to provide moist environment to the wound and replaced by modern dressings with more advanced formulations<sup>12</sup>.

Modern wound dressings were developed in the 20th century<sup>13</sup>. In the mid-1980s, the first modern wound dressing was developed to provide critical features including moisture retention and fluid absorption. Synthetic wound dressings now include multiple products such as hydrogels, tissue adhesives, foams, vapor-permeable films, alginates, and silicone meshes<sup>11</sup>. All of these new products were designed with moist wound healing in mind, seeking the ‘Holy Grail’ of healing<sup>14</sup>.

Plethora of wound dressings have been developed, based on their origin as natural or synthetic. Natural wound dressings are fabricated with natural polymers, typically including cellulose<sup>15</sup>, alginate<sup>16</sup>, chitin and chitosan<sup>17</sup>, collagen<sup>18</sup> and hyaluronic acid<sup>19</sup> because these biopolymers exhibit the ability to control wound exudate and establish a moist environment that promotes wound healing. They were fabricated in various physical forms such as membranes, hydrogels, fibers, and sponges to explore their highest possible efficacy<sup>20</sup>. For instance, a hydrogel was synthesized by UV cross-linking cellulose and acrylic acid, to improve burn wound healing by promoting neovascularization and re-epithelialization<sup>21</sup>. Furthermore, Tangpasuthadol et al. prepared heterogeneous hydrogels modified with stearyl groups in chitosan films to increase protein adsorption. When films reacted with succinic anhydride phthalic anhydride, they became more hydrophilic, and they promoted lysozyme adsorption<sup>22</sup>.

Moreover, to natural wound dressings, synthetic wound dressings, have been developed. Synthetic polymers are biocompatible and bioresorbable with reproducible properties that can be adapted to particular applications. The key difference in synthetic and natural polymer is that the former can be developed and modified in a controlled manner to acquire certain properties and stability. Some of the synthetic polymers used in wound dressings include poly(ethylene glycol) (PEG), poly( $\epsilon$ -caprolactone) (PCL), polyurethane (PU), poly(lactic acid) (PLA), and poly(glycolic

acid) (PGA), and poly(vinyl alcohol) (PVA)<sup>23</sup>. By immobilizing biomolecules such as polysaccharides, adhesion proteins, or peptide sequences on the surface or inside their structure, they can be functionalized to confer the quality of bioactivity<sup>24</sup>. One such example of bioactive synthetic polymer chronic wound dressing is PU hydrogel composites encapsulate with fibroblast growth factor-2, which demonstrate positive *in-vivo* outcomes because of the excellent angiogenic properties of fibroblast growth factor-2<sup>25</sup>.

### 1.3 Proteins in wound healing

Proteins are large, complex molecules essential for the structure, function, and regulation of cells, tissues, and organs. Proteins are composed of amino acids, similar to beads in a string. There are specific sequences in proteins which determine their unique three-dimensional structure and function. There are 20 amino acids that can combine in various ways, forming a diverse array of proteins, each with distinct roles in biological processes. Proteins are involved in nearly every cellular function, including healing, as they play key roles in tissue repair, cell signaling, immune response, and the formation of new blood vessels, ensuring the restoration of damaged tissues<sup>26</sup>.

#### 1.3.1 Subcategories of proteins in wound healing

**Collagen** is the most abundant protein in the human body and provides structural support by creating a framework for the new issue during wound healing. The different phases of wound healing require different forms of collagen, with type I collagen playing the most significant role during the remodelling phase<sup>27, 28</sup>.

**Cytokines** are small proteins that control inflammation and immunological responses, by directing the recruitment of immune cells to the wound site and assisting in the clearance of debris. They help regulate the early inflammatory response to injury<sup>29</sup>. Tumor necrosis factor (TNF) and interleukins are important cytokines in wound healing.

**Fibrinogen** is transformed into fibrin<sup>30</sup> during the first stage of wound healing, resulting in a clot that stops the bleeding. In addition to regulating bleeding, these clotting proteins offer a structure for tissue development and cell migration into the wound<sup>31</sup>.

**Growth Factors (GF)** are a class of naturally occurring proteins or hormones, essential for controlling a number of cellular functions, such as cell division, growth, proliferation, migration,

and survival<sup>32</sup>. They function as signaling molecules that attach to particular target cell surface receptors, starting a chain of intracellular processes that affect cell behavior, examples include epidermal growth factor (EGF), platelet-derived growth factor (PDGF), and vascular endothelial growth factor (VEGF) etc. These GFs are necessary for tissue regeneration and repair as well as angiogenesis, the formation of new blood vessels<sup>33</sup>.

### **1.3.2 Vascular endothelial growth factor (VEGF)**

VEGF, a homodimer 34-46 kDa heparin-binding glycoprotein (116-118), is structurally similar to placental growth factor and PDGF (116) and is highly conserved. VEGF is regarded as one of the most significant GF in wounds due to its pivotal role in angiogenesis<sup>34</sup>, which provides the necessary blood supply to the healing tissue. In turn, this facilitates the effective migration of important cells to the wound site, supports cellular processes necessary for tissue regeneration<sup>35</sup>, and aids in the regulation of the inflammatory response. The healing process would be considerably delayed or compromised in the absence of VEGF<sup>34</sup>. The physiological VEGF growth factors are VEGF-A/B/C/D and placental growth factor<sup>36</sup>. VEGF-A, which has been studied most extensively, is a dimeric 36-46 kD glycosylated protein with an N-terminal signal sequence and a heparin-binding domain. In humans, four different VEGF-A isoforms have been identified with varying numbers of amino acids: VEGF-A<sub>121</sub>, VEGF-A<sub>165</sub>, VEGF-A<sub>189</sub> and VEGF-A<sub>206</sub><sup>37</sup>. These homodimers vary in size and their capacity to bind to heparin, heparan sulfate, or neuropilins-accessory transmembrane proteins. This binding regulates their infusibility and local activity<sup>38</sup>.

One such isoform is VEGF-A<sub>165</sub> (the mature and processed form of which contains 165 amino acid residues) is the predominantly expressed isoform in humans followed by VEGF-A<sub>121</sub> and VEGF-A<sub>189</sub><sup>38</sup>.

One of the studies showed the potential of VEGF in angiogenesis, where prepared chitosan-hyaluronic acid/VEGF loaded nanofibrin composite sponges have potential to induce angiogenesis in wound healing<sup>39</sup>. Not only one cargo but multi-cargo approaches have also been considered in exogenous growth factor therapies. For instance, Poala Losi et al, synthesized fibrin-based scaffold incorporating VEGF and basic fibroblast growth factor (bFGF)-loaded nanoparticles stimulates wound healing in diabetic mice, scaffolds containing GF's induced complete re-epithelialization with enhanced granulation tissue formation/maturity and collagen deposition compared to the

other groups, as revealed by histological analysis suggested its potential use as a dressing in patients with diabetic foot ulcers<sup>40</sup>.

#### 1.4 Challenges in direct delivery of proteins

Irrespective of their impeccable properties, GFs are typical proteins, difficult to administer to the human body because of their short half-lives, large sizes, slow tissue penetration, and potential toxicity at high systemic levels<sup>41</sup>. Figure 1.2 illustrates some limitations of administrative routes for direct delivery of GFs in the human body.

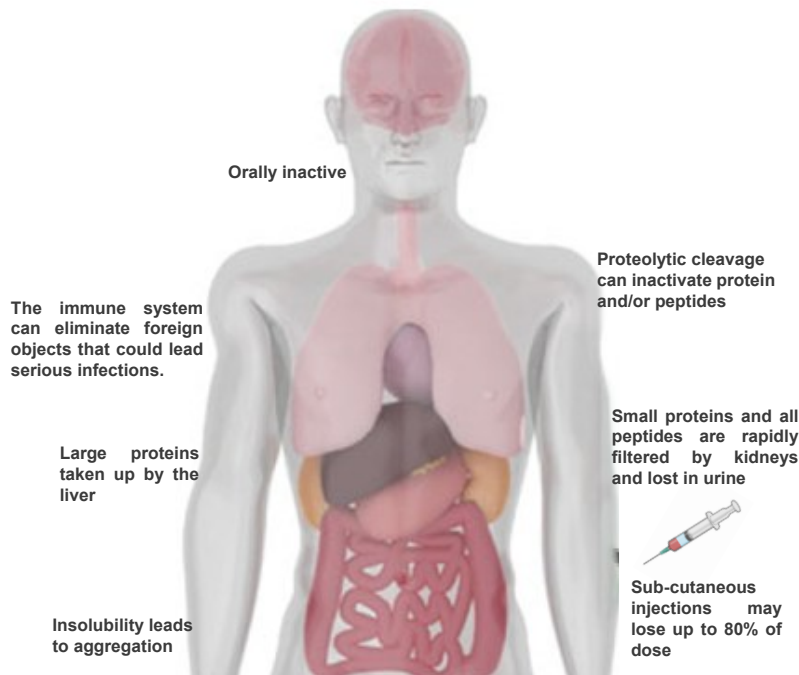


**Figure 1.2** Schematic representation of limitations in direct delivery of growth factors, the human body illustration is created with Biorendor.

As depicted in Figure 1.3, to overcome those drawbacks for GF, three distinct methods have been explored including: physical, bioaffinity and covalent attachment<sup>42</sup>.

##### 1.4.1 Physical encapsulation

This method is simple to incorporate GFs into a three-dimensional (3D) polymer matrix by integrating GFs before solidification or gelation. This method preserves the bioactivity of GFs and

ensures the scaffold's optimized properties remain largely unaffected. Freeman et al, (46) synthesized alginate-sulfate/alginate scaffolds that incorporated VEGF, platelet-derived growth factor-BB (PDGF-BB), and transforming growth factor-beta 1 (TGF- $\beta$ 1), binding them with an affinity similar to heparin for sequential delivery. The results showed improved vascularization in triple-factor scaffolds compared to single-factor ones in rat implants. However, this approach is inefficient, as only a small fraction of GFs can be bound, and their release profiles are unpredictable<sup>43</sup>. Over the past two decades, physical immobilization of GFs onto matrices has gained attention due to its simplicity and mild conditions. However, it often leads to inefficient retention of soluble proteins and poorly controlled delivery. Ziegler et al, found that when bone morphogenetic protein-2 (BMP-2) and bFGF were physically immobilized on synthetic bone implants, both GFs lost their biological activity after an initial burst on the surfaces *in vitro*<sup>44</sup>. These studies highlight the need for more advanced methods to enhance the immobilization of GFs on implant surfaces or their encapsulation within carriers for improved long-term retention.

#### **1.4.2 Bioaffinity GF immobilization**

This method has been developed for an optimal delivery system in a highly spatiotemporal regulated manner, further imitating extra cellular matrix (ECM) functions, drawing inspiration from the natural interactions between ECM and GFs. The ECM is a dynamic microenvironment that regulates cellular processes and acts as a reservoir for GFs due to their high-affinity binding to molecules. GFs like BMP-2, BMP-7, VEGF, PDGF, and FGF-2 interact with heparan sulfate in the ECM<sup>45, 46</sup>. To enhance GF delivery, biomaterials are often decorated with heparin or heparin sulfate-mimetic molecules, sequestering their binding ability. For instance, Jha et al,<sup>47</sup> developed heparin-functionalized hyaluronic acid-based hydrogels to study the effect of heparin molecular weight (MW) and concentration on TGF $\beta$ 1 loading and retention. High MW heparin improved TGF $\beta$ 1 loading, retention, and slow release due to its stronger affinity for TGF $\beta$ 1. Additionally, GF binding to high MW heparin hydrogels enhanced stem cell differentiation into endothelial cells, promoting vascular-like network formation. This technique offers enhanced biological activity but comes with several limitations. First, weak binding leads to limited retention, causing early release and loss of bioactivity<sup>48</sup>. Second, unpredictable release kinetics often result in an initial burst, reducing therapeutic effectiveness<sup>48</sup>. Third, immobilization can interfere with the

natural binding sites or conformation of GFs, diminishing their biological activity and hindering target cell interactions<sup>49</sup>.

### 1.4.3 Covalent attachment

This method prevents the risk of an initial burst release, making it a promising strategy for enhancing the stability and persistence of GFs when administered to cells or tissues<sup>50</sup>. Covalent attachment is crucial when biomolecules cannot adsorb onto substrate surfaces or when GFs are weakly adsorbed due to improper orientation. In contrast, covalent binding of GFs typically involves chemical or enzymatic interactions between proteins and functionalized surfaces, offering precise control over the amount, orientation, retention, and distribution of GFs within solid matrices. This method facilitates localized and sustained GF delivery. Chemical binding regulates GF desorption through enzymatic or hydrolytic cleavage of the covalent bond, enabling customized release profiles (linear, pulsatile, or sequential). Furthermore, covalent attachment enhances GF stability, reduces protein requirements, and improves therapeutic efficacy, promoting tissue regeneration while reducing costs<sup>51</sup>. There are several strategies for modifying proteins to enhance their stability and insolubility, enabling the use of lower doses to achieve similar biological effects. Covalent attachment relies on the availability of specific amino acids in GFs that can form chemical bonds with reactive polymers bearing functional groups. For example, carbodiimide group has an affinity for amine or carboxyl groups, while succinimidyl ester and phenylazide derivatives are commonly used for their affinity towards the amino groups of proteins<sup>50</sup>. One such strategy to modify the protein using polymer is PEGylation.

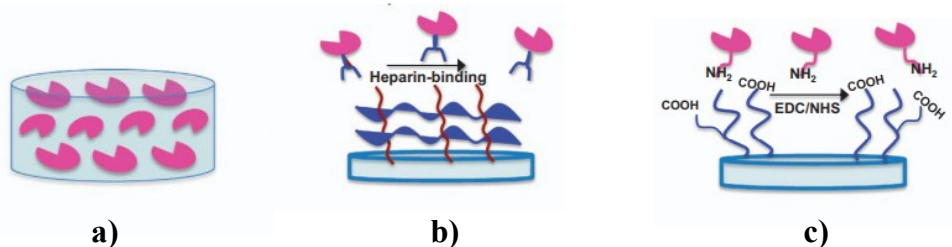


**Figure 1.3** Schematic illustration for delivery of GF's, including (a) physical encapsulation, (b) bioaffinity, and (c) covalent attachment<sup>51</sup>. Copyright 2017, Nature Publishing Group.

## 1.5 Approaches to synthesize polymer-protein bioconjugates

Figure 1.4 illustrates three distinct approaches, including grafting to, grafting from, and grafting through.

### 1.5.1 Grafting to

This method involves the initial synthesis of end-functionalized polymers, which are then conjugated to the protein *via* a chemical reaction. However, the method often suffers from low conversion efficiency due to steric hindrance and the limited availability of reactive groups<sup>52</sup>. Therefore, to compensate, an excess of polymer is usually required, leading to the need for an additional purification step to remove any unbound polymer<sup>53</sup>. While this method is considered as widely used and straightforward<sup>54</sup>, because polymerization stages are separated from the conjugation step, enabling a wider range of reaction conditions for synthetic polymerization schemes that might not be compatible with proteins and provides control over polymer structure for various applications. However, it is limited by low yield and challenges in purifying the final product from unreacted reagents<sup>55</sup>.

### 1.5.2 Grafting from

This method involves initiating polymerization directly from the protein surface, resulting in well-controlled protein-polymer conjugates<sup>56</sup>. A low molecular weight initiator is first bioconjugate to the protein, allowing the polymer chain to grow from the protein-bound initiator. This approach leverages advanced living polymerization techniques<sup>57</sup>, such as controlled radical polymerization (CRP), including Reversible Addition-Fragmentation Chain Transfer (RAFT) and Atom Transfer Radical Polymerization (ATRP), to achieve efficient conjugation between small molecules and proteins. The method ensures high yield and faster purification, as small monomers and catalysts can be easily separated from the resulting protein-polymer conjugates<sup>58</sup>. However, it requires precise control of polymerization conditions such as solvent, temperature and could be limited by the protein's structure or accessibility for initiator attachment.

### 1.5.3 Grafting-through

This method involves the synthesis of macromonomers with the protein as pendant group. The macromonomers then undergo further polymerization or post-polymerization conjugation,

attaching multiple protein molecules to a polymer chain, resulting in a high-density protein structure with a comb-like shape. However, the relatively low polymerization degree and the complexity of the resulting product make this method less commonly used<sup>59, 60</sup>.

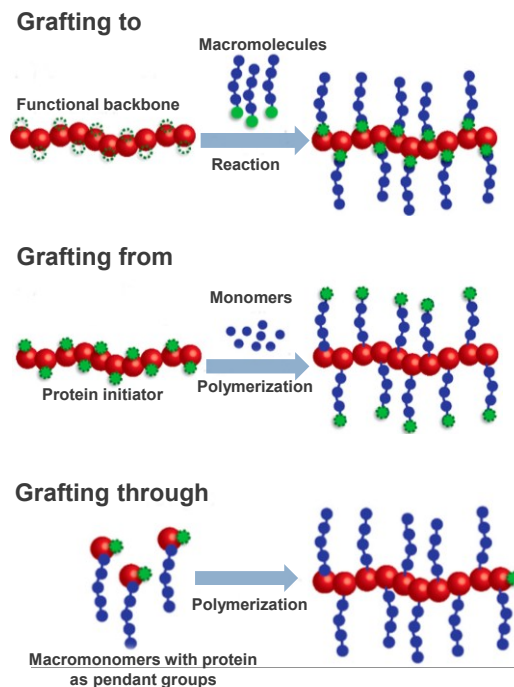


**Figure 1.4** Schematic illustration of three distinct approaches to synthesize polymer-protein bioconjugates<sup>61</sup>. Copyright 2019, American Chemical Society.

## 1.6 PEGylation of proteins

PEGylation refers to the covalent attachment of poly(ethylene glycol) (PEG) to biomolecules, such as proteins, peptides, or drug molecules. Such modification enhances the stability, solubility, bioavailability, and blood circulation time of biomolecules<sup>62</sup>. Additionally, PEGylation could improve the immunogenicity and susceptibility of biomolecules to proteolytic degradation of proteins, thereby improving their suitability for therapeutic use<sup>63</sup>.

For covalent conjugation of PEG to proteins, facile click-type reactions have been investigated, Figure 1.5 summarizes common strategies to modify proteins with respects to specific sites of proteins and functionalization of PEG chains through the modification reactions;

acylation, alkylation, redox reactions, and aromatic ring substitution. The specific sites in proteins include sulfhydryl groups in cysteine (Cys) residues<sup>64, 65</sup>, an amino group in lysine (Lys)<sup>64, 66</sup> residue, and carboxylic acid group in glutamine (Glu) residue in side chains. In addition, they also include terminal amino and carboxylic acid groups<sup>67</sup>.

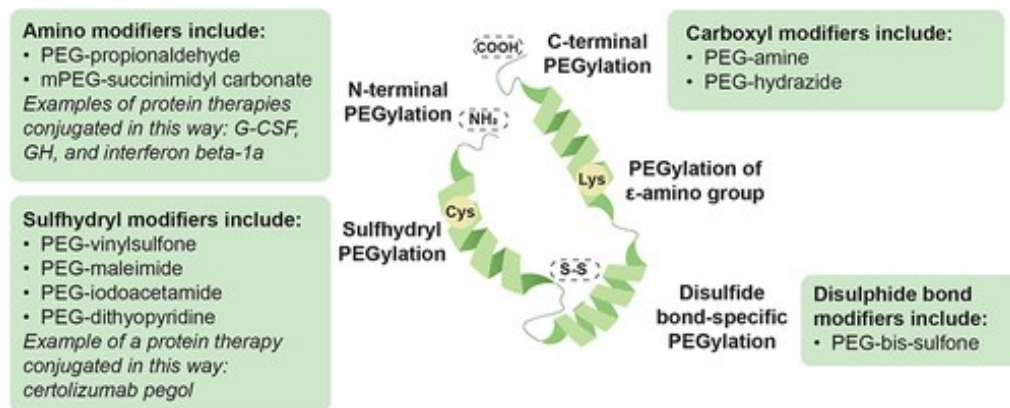


**Figure 1.5** Schematic illustration of specific sites in proteins for covalent attachment<sup>64</sup>.

Copyright 2024, Frontiers.

One of the examples of selective PEGylation involves conjugating the polymer to the thiol groups of Cys residues<sup>63</sup>. In most proteins, Cys is involved in disulfide bonds (Cys-Cys) that stabilize the protein's structure, while in a few cases, free Cys plays a biological role<sup>68</sup>. PEGylation of Cys is achieved using activated PEGs that specifically react with thiol groups<sup>69</sup>, such as PEG-vinyl sulfone, PEG-iodoacetamide, PEG-dithiopyridine, and PEG-maleimide<sup>65</sup>. These functional groups preferentially react with Cys, forming polymer-protein bonds with varying stabilities. An example is certolizumab pegol, a PEGylated TNF-alpha inhibitor Fab' fragment, synthesized via free Cys PEGylation with 40 kDa (2×20 kDa PEG chains) of branched PEG-maleimide<sup>70, 71</sup>. Additionally, PEG-orthopyridyl disulfide specifically reacts with sulfhydryl groups<sup>66</sup>.

## 1.7 Type of delivery vehicles in wound healing applications

A wide range of wound dressings have been developed to address different aspects of the wound healing process and diversity of wound types. An ideal dressing (Figure 1.6) should achieve rapid healing at reasonable cost with minimal inconvenience to the patient<sup>72</sup>. Typically, wound

dressings are classified in two categories as traditional or modern (moist wound environment) as mentioned earlier in Section 1.2. When it comes to chronic wounds, modern dressings are classified not only for healing capabilities but also for their ability to retain moisture<sup>12</sup>. This includes materials such as foam and spongy scaffolds, nanofibrous matrices, hydrogels and films. These delivery vehicles can be combined with GF's or other biomolecules to enhance healing, making them bioactive wound dressings<sup>73</sup>.



**Figure 1.6** Schematic illustration of an ideal wound dressing<sup>72</sup>. Copyright 2022, MDPI.

### 1.7.1 Foam and spongy scaffolds

Spongy biomaterial structures, typically created by freezing and subsequent lyophilization of solutions, have been extensively studied for wound healing applications. Their substantial pore size, ranging from 50  $\mu\text{m}$  to several millimeters, plays a crucial role in supporting cellular infiltration, migration, and signaling<sup>74</sup>. The pore structure and size distribution can be tailored by adjusting the concentration of materials or the parameters of the freeze-drying process. Due to their high porosity, well-connected pore networks, excellent fluid retention capabilities, and oxygen permeability, sponges have proven effective in treating various types of chronic leg ulcers. One of the key advantages of these sponges is their ability to maintain a physiologically moist environment, thereby promoting granulation tissue formation<sup>75</sup>.

Biomaterials derived from natural sources, such as collagen, gelatin, chitosan, and alginate are commonly employed to fabricate sponges for wound healing purposes. Collagen-based sponges

are particularly favored due to their superior mechanical and physicochemical properties, which help prevent wound contraction and facilitate fluid absorption. These sponges support cell adhesion, migration, and proliferation of fibroblasts and keratinocytes on their surface<sup>75</sup>. However, the limited antimicrobial properties of collagen led to the development of collagen sponges loaded with anti-infective bioactive agents, as proposed by Ramanathan, which enhanced collagen deposition, growth factor expression, and re-epithelialization even after 14 days of application<sup>75</sup>.

A significant drawback of traditional collagen, primarily sourced from porcine or bovine tissues, is its rapid degradation and the potential risk of transmitting zoonotic diseases. Consequently, fish collagen and gelatin have gained attention as alternative materials for wound dressings. Chandika et al, successfully designed a fish collagen-based sponge scaffold crosslinked with sodium alginate and chito-oligosaccharides, resulting in biocompatible, stiff structures with lower biodegradability<sup>76</sup>. Gelatin, known for its favorable degradation profile and angiogenic properties, helps avoid the drawbacks associated with collagen. However, its porosity and water absorption characteristics are less optimal compared to other naturally derived hydrogels, such as hyaluronic acid, chitosan, or alginate. Additionally, gelatin is often combined with chitosan to enhance its antibacterial and hemostatic properties. Despite these improvements, studies indicate that gelatin's high diffusivity limits the effectiveness of growth factor retention and reduces the long-term stability of biomolecules<sup>77</sup>. To address these issues, Jinno et al, proposed a sponge scaffold incorporating 10% acidic gelatin, which preserved the positive charge of FGF. By optimizing the release rate and formulation of the gelatin scaffold, they demonstrated that 7  $\mu\text{g}/\text{cm}^2$  of FGF could significantly accelerate wound healing and promote vascularization<sup>78</sup>.

In general, sponges offer larger pore sizes than hydrogel scaffolds, facilitating cellular ingrowth. However, these large pores can negatively influence the mechanical properties and swelling behavior of the material, requiring careful engineering of the scaffold composition to ensure these properties are controlled during the healing process. Furthermore, the large pores of spongy materials can lead to the rapid dispersion of encapsulated drugs and GF's. Despite these challenges, fibrous and hydrogel scaffolds have garnered more attention for developing scaffolds that better support wound healing.

### 1.7.2 Nanofibrous matrices

Fibrous scaffolds have garnered significant attention in the field of wound healing due to their ability to influence cell alignment, morphology, and function by replicating the structure of the ECM<sup>79</sup>. These nanofibrous scaffolds can be fabricated using various methods<sup>80</sup>, including self-assembly, phase separation, and electrospinning, with electrospinning being considered the most promising technique<sup>81</sup>. This method employs an electrical field to charge a polymeric solution, which is then ejected from a syringe and collected onto a grounded metallic plate<sup>82</sup>. The resulting electrospun nanofibers have a high surface area to volume ratio, interconnected pores, and fiber diameters ranging from 10 to 100 nm, which effectively mimic the native ECM structure<sup>83</sup>. Additionally, electrospun matrices exhibit desirable properties such as oxygen permeability, fluid exchange without accumulation, suturability, and uniform in situ adherence, making them desirable for wound healing applications<sup>84, 85</sup>. Electrospun nanofibers made from natural proteins like gelatin and gelatin methacryloyl (GelMA) have shown promising results when implanted in wound models, significantly accelerating wound healing by reducing necrosis and promoting vascularization<sup>86</sup>.

Fibrous scaffolds for skin substitutes are often made from synthetic polymers such as polycaprolactone (PCL)<sup>83</sup>, poly(L-lactic acid) (PLLA)<sup>87</sup>, and poly(L-lactic acid-co-glycolic acid) (PLGA)<sup>88</sup>. Natural polymers like gelatin<sup>79</sup>, chitosan<sup>89</sup>, and collagen<sup>88</sup> are also commonly incorporated into these scaffolds. For instance, Chandrasekaran et al. developed a biocompatible electrospun scaffold from a poly(L-lactic acid)-co-poly( $\epsilon$ -caprolactone) (PLACL) blend combined with gelatin<sup>79</sup>. They showed that plasma surface treatment enhances the scaffold's hydrophilicity, cell proliferation and collagen deposition<sup>79</sup>. Similarly, electrospun chitosan-based scaffolds<sup>90</sup> have been explored for wound healing applications due to their antibacterial properties, hemostatic effects, and ability to support fibroblast adhesion and proliferation *in vitro*, as well as to promote wound healing *in vivo*.

In recent studies, the encapsulation of bioactive molecules within synthetic polymeric nanofibers has been investigated to improve the biological performance of these materials, overcoming the lack of cell-recognition sites inherent in synthetic polymers<sup>83, 91</sup>. For example, PCL-PEG copolymers were electrospun, soaked in recombinant human epidermal growth factor (rhEGF), and functionalized using (1-ethyl-3-(3-dimethylaminopropyl) carbodiimide) to graft the

GF, to enhance wound healing in animal models<sup>92</sup>. Furthermore, anesthetics for pain relief and antibiotics like ampicillin have also been incorporated into electrospun scaffolds for infection management<sup>82</sup>. In another study, an angiogenic peptide, vasoactive intestinal peptide (VIP), was encapsulated in situ in PCL nanofibers by coating them with mussel-inspired dopamine (DA) to create a highly adhesive layer. The VIP was then loaded as microspheres within the PCL/DA nanofiber structure, for a sustained release over 5 days, which significantly enhanced wound healing and angiogenesis in mice with full-thickness wounds<sup>93</sup>.

Electrospun scaffolds have demonstrated the ability to preserve the activity of incorporated drugs over extended periods, with gradual drug release profiles ranging from days to months. Their ECM-like structure and drug delivery capabilities make them highly suitable for skin regeneration applications. However, a significant challenge for electrospun scaffolds is their small pore size, typically less than 10  $\mu\text{m}$ , which limits cell infiltration and ingrowth. Efforts to create scaffolds with larger pore sizes (greater than 20  $\mu\text{m}$ ) are ongoing, as this remains an active research area aimed at improving the controllability of the electrospinning process<sup>94</sup>.

### **1.7.3 Hydrogels**

Hydrogels are the most promising materials for designing scaffolds that promote wound healing<sup>11,95</sup>, as their intrinsic porous hydrophilic structure guarantees gas exchange, fluid balance, controlling water evaporation, absorbing exudate, and providing moisture to the wound area. Moreover, their transparency is an interesting aspect for monitoring regeneration. Hydrogels can mimic the ECM structure and functionality, promoting cell adhesion, proliferation, and directing cell migration<sup>96</sup>. The hydrogel composition influences cell growth, migration, and maturation<sup>97,98</sup>. Hydrogels can also encapsulate bioactive molecules such as drugs<sup>99</sup> and GFs through methods such as physical impregnation or covalent linking to the hydrogel matrix, enhancing tissue regeneration<sup>100</sup>. One of the key properties of hydrogels is their injectability and in situ formation, allowing for minimally invasive scaffold implantation during surgery. Recent advances in adhesive hydrogels, such as GelMA and elastin-based adhesives are degradable and offer up to 20 times the adhesiveness of commercial fibrin glue. With abundant collagen and elastin in the skin ECM, these hydrogels are promising for skin regeneration, focused on improving drug retention and controlled release profiles<sup>101,102</sup>.

Hydrogels are used in various forms, including amorphous gels, solid sheets, or films. Examples of these include products like Nu-gel™ (Johnson & Johnson) and Purilon™ (Coloplast), are hydrogel/alginate combinations. These materials are typically crosslinked to physically trap water, allowing the sheets to absorb and retain significant volumes of water. This makes them particularly useful in wound care, to maintain moisture and support the healing process. Hydrogel dressings generally contain 70–90% water, making them effective at rehydrating dry or necrotic wounds, though they are best suited for light to moderately exuding wounds. As illustrated in Figure 1.7, these dressings offer several benefits, including being non-reactive with biological tissue, permeable to metabolites, non-irritating, and promoting moist healing<sup>103</sup>, illustrating most of the essential characteristics of an "ideal dressing"<sup>104</sup>. These properties help accelerate healing<sup>105</sup>, provide pain relief making them highly acceptable to patients.

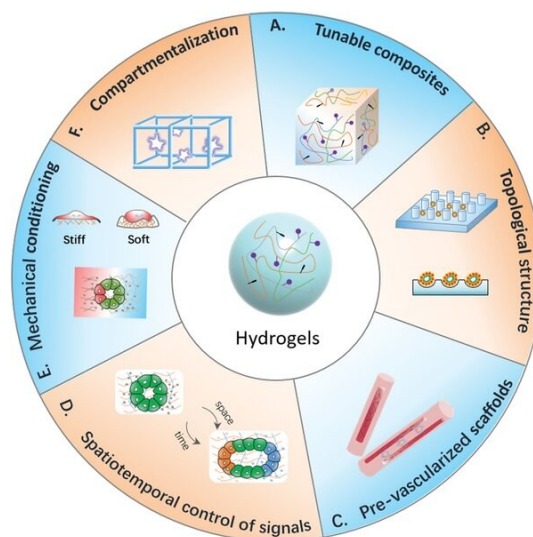


**Figure 1.7** Typical characteristic features of a hydrogel<sup>106</sup>. Copyright 2019, Wiley.

Hydrogels are further categorized as natural or synthetic based on their origin<sup>107</sup>. Natural hydrogels dressings<sup>108</sup> have attracted significant attention in wound healing applications because of their excellent biocompatibility and ability to mimic the ECM, thereby supporting tissue regeneration. Various naturally derived materials, such as fibrin, chitosan, dextran, and alginate, have been explored for their potential in hydrogel formulations<sup>108</sup>.

Fibrin-based hydrogels have shown great promise in wound healing due to their ability to promote vascularization and cell recruitment, essential for tissue repair<sup>100</sup>. These hydrogels are often used in combination with growth factors like rhEGF to maintain sustained release of GF's, enhancing wound closure. However, challenges such as slow crosslinking and potential immune responses can limit their widespread application<sup>109</sup>.

Chitosan-based hydrogels<sup>96</sup> are favored for their antimicrobial properties and their ability to support cell adhesion, migration, and differentiation, which are critical for wound healing. Additionally, dextran-based hydrogels have been modified with amine groups by Sun et al, to improve adhesion and integration on the wound site to improve angiogenesis by facilitating tissue regeneration<sup>110</sup>. In clinical applications, carboxymethylcellulose-based hydrogels have been FDA-approved for the delivery of PDGF (becaplermin) in the treatment of diabetic neuropathic ulcers. Chitosan and alginate-based hydrogels are also gaining attention for their ability to promote re-epithelialization and collagen deposition, which are considered as crucial steps in wound healing<sup>111</sup>. Alginate, derived from brown algae, is widely used due to its biocompatibility, biodegradability and capacity to form hydrogels suitable for tissue regeneration, solidifying the role of natural hydrogels in advancing wound care<sup>16</sup>. Although natural hydrogel dressings are biocompatible and cost-effective, they suffer from batch-to-batch variability, limited control over properties and shorter shelf life. As a result, synthetic dressings were developed, offering the advantage of tunable properties and eliminating batch-to-batch variability.

In contrast, synthetic hydrogels, such as those made from PCL, PLLA, PLGA and PVA, offer the advantage of tunable mechanical properties and degradation rates<sup>112</sup>. Synthetic hydrogels often lack cell recognition sites, limiting their biological properties, thereby recent advancements focus on incorporating bioactive molecules into these hydrogels to improve cell compatibility and tissue regeneration. For example, hydrogel dressings for delivering TGF- $\beta$ 1, showed improved wound healing outcomes<sup>113, 114</sup>.

Additionally, synthetic hydrogels have been developed to improve drug release profiles and serve as delivery systems for various therapeutic agents. Hydroxypropylcellulose (HPC) and biodegradable gelatin hydrogels have been utilized for GF delivery in tissue regeneration, such as FGF-2 for periodontal tissue repair<sup>115</sup>. In order to control burst release of GFs in hydrogels, various strategies have been employed on GF's itself, such as modifying their charge<sup>116</sup> or higher heparin

content<sup>117</sup>, so that heparin binding GF'S can be readily loaded in the hydrogel to improve loading and sustain release. Moreover, biodegradable in situ thermosensitive hydrogels, such as PEG-PCL-PEG incorporating curcumin-loaded micelles, have been developed to improve wound healing by enhancing tensile strength and promoting better wound closure in models<sup>118</sup>.

Furthermore, pH-sensitive hydrogels, such as Poly(N-isopropylacrylamide-co-acrylic acid) have been evaluated for sustained release of biomolecules like bovine serum albumin (BSA), VEGF, and EGF. It showed better healing responses when compared to non-stimulus GF delivery systems<sup>119</sup>.

## **1.8 PVA-based and boronic ester-crosslinked hydrogels**

### **1.8.1 PVA-based hydrogels**

PVA has been extensively studied for wound healing due to its excellent water solubility, biocompatibility, biodegradability, non-carcinogenicity, mechanical properties, and easy processability<sup>120</sup>. PVA-based hydrogels accelerate healing by delivering drugs, GFs, and other proteins. Beyond the advantages of typical hydrogel materials (ability to absorb water, gas permeability, soft tissue imitation, flexibility and biocompatibility), PVA-based hydrogels are distinguished by their good mechanical properties and the ability to retain water in the structure, which ensures a prolonged moist environment<sup>121-123</sup>.

The preparation of PVA-based hydrogels can be broadly categorized into two main methods: physical crosslinking and chemical crosslinking. Crosslinking is essential for ensuring the effective delivery of bioactive molecules and overcoming the inherent water solubility of PVA. This process imparts crucial structural stability and elasticity to the hydrogel, enabling it to swell appropriately when exposed to water or biological fluids<sup>124-126</sup>.

Physical crosslinks could be typically achieved through various supramolecular interactions, including ionic interactions, crystallization, stereocomplexation, hydrophobic interaction, protein interactions, and hydrogen bonding<sup>127</sup>. On the other hand, chemical crosslinking involves the formation of covalent bonds between different macromolecules. This approach is commonly employed to enhance PVA properties, making it suitable for a wide range of applications including wound dressings and drug delivery. Chemical crosslinking reduces the hydrophilic nature of PVA by diminishing the number of hydroxyl groups, resulting in a network structure that is insoluble in

water or other solvents but can swell and absorb large amounts of water or small molecules. Chemical crosslinking can be achieved through classical reactions such as esterification, etherification, carbamation, or radical polymerization, as well as modern methods like click chemistry, bioconjugation, and dynamic bond formation<sup>128-130</sup>.

### 1.8.2 Boronic ester-crosslinked hydrogels

Boronic ester (BE) crosslinked hydrogels combine the benefits of both boronic acid (BA) and hydrogel materials. Beyond structural stability from crosslinking, the inclusion of BE enhances the hydrogel with unique properties, such as stimuli-responsiveness, reversibility, and self-healing abilities. At the same time, the 3D network structure and swelling characteristics of the hydrogel play a crucial role in supporting and amplifying the diverse functions of boronic acid.

Several crosslinkers have been reported to form BE crosslinks to fabricate BE crosslinked hydrogels. Figure 1.8 shows the examples of diboronic acid crosslinkers in literature including boric acid (borax)<sup>131</sup>, and aromatic diboronic acids, such as benzene-1,3-diboronic acid (1,3-BDB), tetrahydroxydiboronic acid (THDB), and 4,4'-biphenyldiboronic acid (4,4'-BPDBA)<sup>132</sup>. Additionally, copolymers with diol groups like poly(N-vinylpyrrolidone-co-3-acrylamidophenylboronic acid)<sup>133</sup>, poly(N,N-dimethylacrylamide-co-N-acryloylm-aminophenylboronic acid)<sup>134</sup> have been synthesized and used to fabricate interpolymer complex hydrogels.

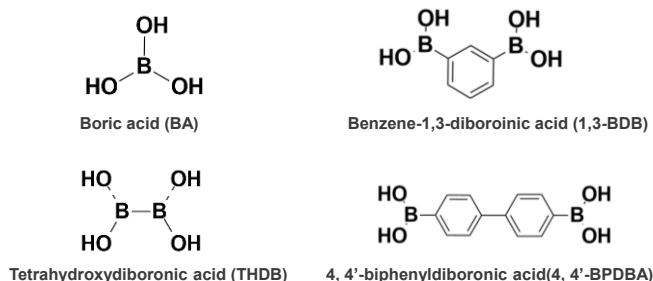


**Figure 1.8** Typical diboronic and boric acid crosslinkers reported in literature.

The formation of hydrogel by mixing PVA solution with borax solution was first reported over six decades ago<sup>131</sup>. Similarly, other polyhydroxy polymers, such as poly(glyceryl methacrylate)<sup>135</sup> and various polysaccharides<sup>136-138</sup>, can also form gels with borax. NMR studies have shown that

$B(OH)_4$  binds to alternating OH groups on the polymer, particularly when they are in meso configuration<sup>139</sup>. Due to the reversible reaction between borate and diol, the borate–polyol gel network is transient. This allows the gel structure to reorganize and self-heal, any mechanical disruption<sup>137, 138</sup>.

Stimuli responsive gels were studied extensively to enhance the release of encapsulated molecules. For example, glucose-responsive hydrogels encapsulating insulin protein were synthesized by Akbar et al, using PVA chains crosslinked with pinacol esters of bisboronic acid *via* a thermodynamically favorable transesterification reaction and entrap insulin as shown in Figure 1.9, where these hydrogels showed a good %release of insulin under stimuli responsive degradation (SRD) conditions<sup>140</sup>.

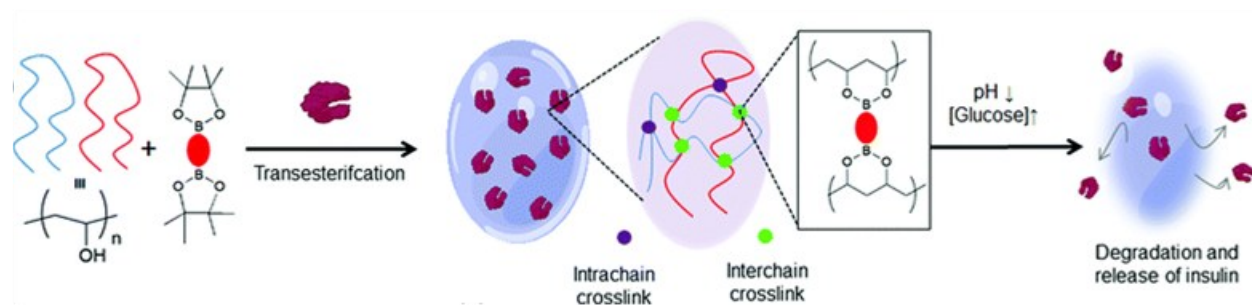


**Figure 1.9** Schematic representation to synthesize glucose-responsive hydrogels crosslinked using bisboronic acid and release of encapsulated insulin under SRD conditions<sup>140</sup>. Copyright 2022, Royal Society of Chemistry.

Ivanov et al,<sup>134</sup> utilized poly(N,N-dimethylacrylamide-co-N-acryloylm-aminophenylboronic acid) to crosslink PVA and discovered that it requires significantly lower boron concentrations compared to borate buffers, with a seven-fold decrease at pH 8.6 and ten-fold at pH 7.5. The interpolymer complex gel formed showed a longer relaxation time than borate–PVA gels, suggesting a more stable crosslink structure. Additionally, these boronate–diol interactions-based gels were glucose-sensitive, allowing glucose to diffuse through them. Similar to borate–polyol gels, the interpolymer complex gels also exhibited pH- and temperature-dependent behaviors as reported by Kiser et al<sup>141-145</sup>.

He et al. developed crosslinked polymeric hydrogels. As illustrated in Figure 1.10, they were fabricated from a mixture of a branched catechol-derivatized poly(ethylene glycol) (cPEG) with BDBA, in 30 min at pH 9.0<sup>146</sup>. Similar to gels created by Kiser et al,<sup>142</sup> the cPEG–BDBA gel exhibited pH responsivity, dissolving gradually when immersed in a pH 7.4 buffer. Notably, the gel demonstrated autonomous and rapid healing when fractured, simply by bringing the fractured surfaces into contact.

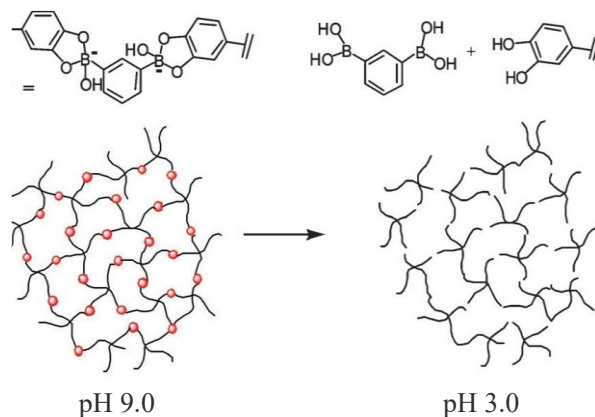


**Figure 1.10** Schematic illustration to fabricate polymeric hydrogels from a mixture of a branched catechol-derivatized poly(ethylene glycol) with BDBA diboronic acid crosslinker<sup>146</sup>. Copyright 2011, Royal Society of Chemistry.

One other example of self-healing hydrogel is Borate bonds-containing pH-responsive chitosan hydrogel synthesized by Yang et al<sup>147</sup>, where the fabrication was done by reacting phenylboronic acid grafted on chitosan with the hydroxyl group of PVA to generate BE bonds as shown in Figure 1.11. The gels were doped with tannic acid (TA)/iron nanocomplex (TAFE) for postoperative tumor recurrence and wound infection prevention. Such self-healing hydrogels have significant potential for applications like wound healing.

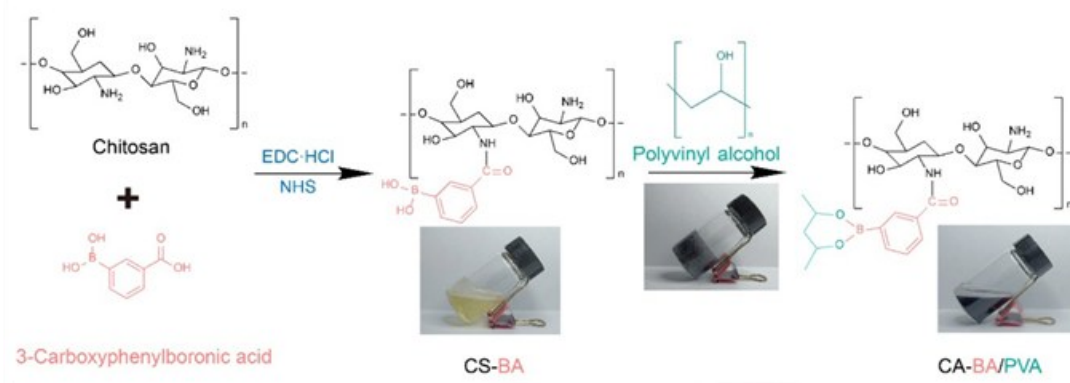


**Figure 1.11** Schematic demonstration of Chitosan/PVA/TAF hydrogel crosslinked with phenylboronic acid<sup>147</sup>. Copyright 2024, Elsevier.

Additionally, aromatic bis-boronic acid crosslinkers such as, 1,4-BDBA and 4,4'-BPDBA, are known to be pH, glucose, and ROS responsive. The use of biocompatible PVA and bis-boronic acid crosslinkers enhances the potential for *in vivo* applications<sup>132</sup>. PVA–tetrahydroxyborate (THB) hydrogels<sup>148</sup> demonstrated superior mechanical and rheological properties, where the concentrations were key factors in determining their rigidity, adhesiveness, and network formation. Increasing THB concentrations enhances the gel's rigidity, while higher PVA molecular weight and hydrolysis contributed to strengthening the hydrogel. These hydrogels offer controlled release properties, as larger PVA molecules limiting the diffusion of components, and boron release with increasing in a non-linear fashion with THB concentration. Temperature also impacts the network formation, with elevated temperatures, rigidity reduced. Overall, PVA–THB hydrogels strike an ideal balance between fluidity, cohesiveness for wound application and extended use, making them highly promising for wound healing and drug delivery applications.

## 1.9 Scope of the thesis

The main objective of my MSc research is to develop BE-crosslinked PVA-based hydrogel films encapsulating PEG-VEGF<sub>165</sub> bioconjugates, promoting healing in chronic wounds. The research focuses on the synthesis, characterization, and encapsulation of PEG-VEGF<sub>165</sub> bioconjugates in THDB-crosslinked PVA hydrogels. Chapter 2 describes experimental methodology. Chapter 3 is dedicated to the results and discussion. A novel synthetic, LF-loaded, pH-responsive THDB-crosslinked PVA hydrogel film was developed for encapsulating

bioconjugates, with the potential to promote cell proliferation and angiogenesis at the injury site, thus accelerating the healing process in chronic wounds. Finally, Chapter 4 presents a summary and suggestions for future research.

This research introduces a novel hydrogel film for wound dressing applications by encapsulating bioconjugates and an anti-microbial drug. The film provides a controlled environment for therapeutic delivery, enhancing wound healing. Its design ensures stability and bioactivity retention of the encapsulated bioconjugates. This innovation holds promise for advanced wound care solutions.

# Experimental and Methods

## 2.1 Experimental

### 2.1.1 Instrumentation

<sup>1</sup>H-NMR spectra were recorded using a 500 MHz Bruker spectrometer. The CDCl<sub>3</sub> singlet at 7.26 ppm was selected as the reference standard. Circular Dichroism spectra were recorded Jasco J-815 CD Spectropolarimeter using 200 μL quartz cuvettes with path length of 1 cm. FT-IR spectra were collected with a Thermo Scientific Nicolet iS5 Spectrometer equipped with an iD5 attenuated total-reflection accessory. UV-Vis spectra were recorded on a Cary 60 UV-Vis Agilent Spectrometer using a disposable PMMA cuvette with an optical path length of 1 cm. The sizes and size distributions of PEG-based precursors and PEG-VEGF<sub>165</sub> bioconjugates in hydrodynamic diameter were measured by dynamic light scattering (DLS) at a fixed scattering angle of 175 ° at 25 °C with a Malvern Instruments Nano S ZEN1600 equipped with a 633 nm He-Ne gas laser. Fluorescence images were analyzed using Nikon Eclipse TiE Inverted Epifluorescence Microscope equipped with six bright lenses and a gas and temperature controlled stagetop incubator.

### 2.1.2 Materials

An aqueous solution of acrylamide/bisacrylamide solution (40% w/v, 99.9%), sodium dodecyl sulfate (SDS, ≥98.5%), ammonium persulfate (APS, ≥98.5%), tetramethyl ethylenediamine (TEMED, 99%), tris base (99.9%), bromophenol blue, t-butanol (≥99.5%), carbonyl diimidazole (CDI, ≥90%), 2,2'-(ethylenedioxy)diethanethiol (DEG-DSH, 95%), 1,8-diazabicyclo[5.4.0]undec-7-ene (DBU, 97.5%), divinyl sulfone (DVS, ≥96%), sodium hydride (NaH, 90%), poly(vinyl alcohol) (PVA with M<sub>w</sub> ≈ 89 – 98 kg/mol, 99%), tetrahydroxydiboronic acid (THDB, 95%), Coomassie brilliant blue G-250 dye, benzene-1,4-diboronic acid (BDB, 95%), boric acid (99.5%) bovine serum albumin (BSA, ≥96%), molecular sieves (pore diameter = 3 Å and bead diameter = 8-12 mesh), aqueous 30 wt% hydrogen peroxide solution, glucose, flourescamine dye (98%), levofloxacin (LF, 96%), phosphate buffered saline (PBS) tablets, muller Hinton Broth 2 (MHB) microbiology culture medium, agar powder (quality level 100) were

purchased from Millipore Sigma, used without any further purification unless otherwise mentioned.

Vascular endothelial growth factor (VEGF<sub>165</sub>, >95%) was purchased from Genscript. As illustrated in Figure 2.1, the protein consists of the sequence of 165 amino acids with 16 cysteine residues (highlighted). Based on the data sheet by manufacturer, three cysteine residues exist as free while six residues exist as three intrachain (52-94, 83-128, 87-130) and two interchain (77, 86) disulfide linkages.

|     | 5                                       | 10 | 15 |
|-----|---|----|----|
| 1   | A P M A E G G G Q N H H E V V K F M D V |    |    |
| 21  | Y Q R S Y C H P I E T L V D I F Q E Y P |    |    |
| 41  | D E I E Y I F K P S C V P L M R C G G C |    |    |
| 61  | C N D E G L E C V P T E E S N I T M Q I |    |    |
| 81  | M R I K P H Q G Q H I G E M S F L Q H N |    |    |
| 101 | K C E C R P K K D R A R Q E N P C G P C |    |    |
| 121 | S E R R K H L F V Q D P Q T C K C S C K |    |    |
| 141 | N T D S R C K A R Q L E L N E R T C R C |    |    |
| 161 | D K P R R                               |    |    |

**Figure 2.1** Sequence and amino acid composition in VEGF<sub>165</sub> obtained using PredictProtein online tool.

### 2.1.3 Synthesis of PEG-VEGF<sub>165</sub> bioconjugates using CDI-mediated coupling reaction

#### 2.1.3.1 Synthesis of PEG-CI

PEG (5.0 g, 1 mmol) was mixed with CDI (1.6 g, 10 mmol) in chloroform (30 mL) containing 3Å molecular sieves (30 mg) in an ice bath for 20 min and then stirred at room temperature for 24 h. The reaction mixture was subjected to vacuum filtration to remove molecular sieves and precipitated from cold diethyl ether (500 mL). The precipitate was isolated by vacuum filtration and then dried in vacuum oven at 60 °C to produce a white powder. Yield = 3.7 g (73.6%).

#### 2.1.3.2 Model reaction of PEG-CI with DEG-DSH

PEG-CI (356 mg, 0.068 mmol) dissolved in DCM (5 mL) was mixed with DEG-DSH (100 mg, 0.54 mmol), and then dropwise mixed with DBU (16 µL, 0.1 mmol) under stirring at room

temperature for 24 hrs. The reaction mixture was precipitated from cold diethyl ether. The precipitate was isolated by vacuum filtration and then dried in vacuum oven at 60 °C to yield a white powder. Yield = 0.3 g (70%).

### **2.1.3.3 Bioconjugation of PEG-CI with VEGF<sub>165</sub>**

Aqueous PEG-CI solution (0.1 mg/mL, 0.06 mL) was mixed with aqueous VEGF<sub>165</sub> solution (0.1 mg/mL, 0.03 mL) at different PEG CI/VEGF<sub>165</sub> w/w ratio as 50/1, 100/1, 200/1, and 300/1 at room temperature for 24 hrs. The resulting mixtures were immediately characterized by gel electrophoresis.

### **2.1.4 Synthesis of PEG-VEGF<sub>165</sub> bioconjugates using DVS-mediated coupling reaction**

#### **2.1.4.1 Synthesis of PEG-VS**

PEG (3 g, 0.6 mmol) in a Schlenk flask was dried in vacuum oven for 3 h to remove residual water molecules and then mixed with molecular sieves (15 mg) in dried DCM (60 mL). NaH (18 mg, 0.6 mmol) was added to the reaction mixture under nitrogen. After the addition of DVS (0.7 g, 6 mmol), the resulting mixture was stirred at room temperature for 48 h under inert atmosphere. The reaction was stopped by exposure to air.

For purification, the mixture was washed with aqueous brine solution by three times and dried with sodium sulfate to remove residual water. After the removal of DCM by a rotary evaporation, the product was precipitated in cold diethyl ether. The precipitate was dried in vacuum oven at 40 °C to yield a white powder. Yield = 3.0 g (81%).

#### **2.1.4.2 Bioconjugation of PEG-VS with VEGF<sub>165</sub>**

Aqueous PEG-VS (0.1 mg/mL, 0.06 mL) was mixed with aqueous VEGF<sub>165</sub> solution (0.1 mg/mL, 0.03 mL) at different PEG-VS/VEGF<sub>165</sub> w/w ratio of 50/1, 200/1, and 300/1 at room temperature for 24 h. After 24 h, the resulting mixtures were characterized for gel electrophoresis.

### **2.1.5 Gel electrophoresis**

To prepare running gels, a mixture containing 1.5 M aqueous tris (1.3 mL), 10% aqueous SDS solution (50 µL), aqueous acrylamide/bisacrylamide solution (2 mL), APS (25 µL), and TEMED (2.5 µL) dissolved in deionized water (1.7 mL) was subjected to polymerization on gel plates at

room temperature for 30 min. Then, stacking gels were prepared from a mixture of 0.5 M aqueous tris (0.62 mL), 10% aqueous SDS solution (25  $\mu$ L), aqueous solution acrylamide/bisacrylamide (0.33 mL), APS (12.5  $\mu$ L), and TEMED (2.5  $\mu$ L) dissolved in deionized water (1.5 mL). t-Butanol (10 mL) was used to align the line of running gel to be straight. After 20 min, excess t-butanol was wiped using a paper towel. The setup for preparing the gel is illustrated in Figure 2.2. Aqueous SDS solution was prepared with 0.5 M aqueous tris HCl solution (pH = 6.8, 1.3 mL), glycerol (2.5 mL), 10% aqueous SDS solution (2 mL), and 0.5% aqueous bromophenol blue solution (0.2 mL) dissolved in deionized water (3.6 mL). Their total volumes were adjusted to 9.5 mL with deionized water. Furthermore, the sample buffer was added in aliquots 30  $\mu$ L each, to the Eppendorf tubes containing the bioconjugates and heated at 95  $^{\circ}$ C for 4 minutes.

Moreover, 10x electrode running buffer pH-8.3, (1 L) was prepared using tris-base (30.3 g), glycine (144 g), and SDS (10 g). Samples were loaded into the small wells of gel plates. The gel ran at 200 V for 1 h, then stained overnight with Coomassie brilliant blue R-250 and destained. Finally, the gel was analyzed under a UV lamp to visualize protein bands.

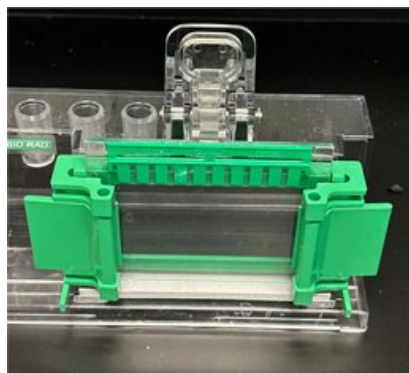


**Figure 2.2** Digital image to show a setup to prepare gels.

## **2.1.6 Fabrication of BE-crosslinked PVA hydrogels**

### **2.1.6.1 General procedure for *in-situ* crosslinking approach**

10% Aqueous PVA solution was prepared by heating a mixture of PVA powder (1 g) in deionized water (10 mL) for 1 h at 80  $^{\circ}$ C. Aliquots were mixed with an aqueous crosslinker solution in a mold to induce THDB-crosslinked PVA hydrogels.

Several parameters that influenced the fabrication of THDB-PVA hydrogels were examined, including various crosslinkers such as THDB, BDB and boric acid, concentration of PVA in water as 0.25, 0.5, 1, 2, 5, and 10% wt, and solvents (DMSO and water) as well as stirring method.

#### **2.1.6.2 General procedure for post-crosslinking approach**

Aqueous PVA solution prepared by heating PVA powder in deionized water for 1 h at 80 °C. Solutions were drop-cast onto flat surfaces and dried in air at room temperature to form PVA films. Their pieces were immersed in a THDB solution (22 mg/mL) for 24 h and then dried in air for 24 h to fabricate THDB-PVA films. They were cut into rectangular shapes with different dimensions.

#### **2.1.6.3 Gel content and swelling ratio**

To estimate %insoluble PVA (or gel content), the films were immersed in deionized water and DMSO for 24 hrs and dried in vacuum oven set at 40 °C for 24 hrs.

#### **2.1.7 Stimuli-responsive degradation of THDB-PVA films**

For pH response, aqueous PBS solutions at different pHs were prepared with 0.2 M aqueous sodium monobasic phosphate solution and 0.2 M aqueous sodium dibasic phosphate solution. Pieces of THDB-PVA films ( $\approx$  100 mg) were incubated in the buffer solutions (100 mL) at different pHs as acidic pH = 5.4, neutral pH = 7.4, and alkali pH = 8.4. Either 1 M NaOH or 1 M HCl was used to adjust pH values. Their weight losses were monitored every 24 h over 6 days.

For hydrogen peroxide response, 1 M aqueous hydrogen peroxide solution was prepared by diluting 30% aqueous hydrogen peroxide solution (25.5 mL) with deionized water to a final volume of 250 mL. Then, pieces of THDB-PVA films ( $\approx$  100 mg) were incubated in the solution (100 mL) and their weight losses were monitored every 24 h over 6 days.

For glucose response, aqueous glucose solution at 1 mg/mL was prepared by dissolving glucose (0.5 g) in deionized water (500 mL). Then, pieces of THBD-PVA films ( $\approx$  100 mg) were incubated in the solution (100 mL) and their weight losses were monitored every 24 h over 6 days.

### **2.1.8 Encapsulation of PEG-VEGF<sub>165</sub> bioconjugates in THDB- PVA films**

A similar procedure to fabricate THDB-PVA films described in Section 2.1.6.2 was applied except for the use of aqueous PEG-VEGF<sub>165</sub> bioconjugate solution. A freshly prepared aqueous PEG-VEGF<sub>165</sub> bioconjugate solution (300/1 w/w ratio, 90  $\mu$ L) was mixed with aqueous 10% PVA solution (1 mL). The resulting mixture was drop-cast in a mold and then dried at room temperature for 24 h. The formed PEG-VEGF<sub>165</sub> bioconjugate-loaded PVA films were then immersed in aqueous THDB crosslinker solution (22 mg/mL) at room temperature for 24 h. The resulting films were isolated and dried in air to fabricate THDB-PVA films embedded with PEG-VEGF<sub>165</sub> bioconjugates films.

### **2.1.9 pH-responsive release of PEG-VEGF<sub>165</sub> bioconjugates using Bradford Assay**

To construct correlation curve, aqueous BSA solution at 0.1 mg/mL was prepared and their aliquots at various volumes as the amount of BSA ranging at 0 - 13  $\mu$ g were mixed with water (1 mL) in disposable UV/vis cuvettes. The results mixtures were mixed with Bradford dye (300  $\mu$ L) and then their volumes were adjusted to be 1.5 mL by addition deionized water. Their UV/Vis spectra were recorded to construct correlation curve with the absorbance at 595 nm. For release experiments, phosphate buffer solutions at acidic pH = 5.4, neutral pH = 7.4, and alkali pH = 8.4 were prepared using 0.2 M aqueous sodium monobasic phosphate and 0.2 M aqueous sodium dibasic phosphate solutions. Their pHs were adjusted using either 1 M NaOH or 1 M HCl. Pieces of THDB-PVA/bioconjugate films (81 $\mu$ g) were incubated in the buffer solutions. Aliquots (1 mL) were taken on a daily basis, the resultant mixtures were mixed with bradford reagent (300  $\mu$ L) and then their volumes were adjusted to be 1.5 mL by addition of deionized water. Their UV/Vis spectra were recorded. The same volumes of fresh buffer solutions were refilled to maintain a sink condition.

### **2.1.10 Fluorescence microscopy to locate bioconjugates in THDB-PVA/bioconjugate films**

Flourescamine dye (6 mg) was dissolved in acetone (1 mL), and further diluted with aqueous PBS solution to obtain the final concentration of 0.5 mg/mL. Sample films (11 mg) were incubated in the prepared flourescamine dye solution (1 mL) for 2 hrs at room temperature and then washed with water (10 mL) twice to remove residual phosphate salts. They were then gently dried using paper towels before microscopy experiment.

### **2.1.11 Fabrication of LF-loaded THDB-PVA/PEG-VEGF films**

A similar procedure for the post-crosslinking approach described in section 2.1.6.2 was applied except for an introduction of LF. A mixture of LF (0.1 g) and PVA (1 g) with water (10 mL) was heated at 80 °C for 1 h to form an aqueous clear (or transparent) solution. Pieces of films ( $\approx$  100 mg) cast in a mold and dried in air were cut in a circular shape (diameter 0.6 cm) and then immersed in aqueous THDB crosslinker solution (22 mg/mL) for 24 h. They were dried in air for 24 h and then further dried in vacuum oven at 60 °C for 2 h. Finally, they were sterilized using a UV lamp light ( $\lambda = 280$  nm) for 2 min.

### **2.1.12 Antimicrobial test with disk diffusion method**

The Kirby-Bauer disk diffusion method was performed in accordance with the European Committee on Antimicrobial Susceptibility Testing (EUCAST) Guidelines. *Escherichia coli* (ATCC 25922) and *Staphylococcus aureus* (ATCC 29213) were seeded into petri dishes containing MHB culture medium (pH  $7.3 \pm 0.2$ , as per the manufacturer's specifications) with inoculum density of 0.5 McFarland Turbidity Standard (approximately  $1-2 \times 10^8$  CFU/mL), via directly suspending colonies. Within 15 minutes of inoculation, disk-shaped LF-loaded THDB-crosslinked/bioconjugate films (9 mm diameter, 0.091 mg) were placed onto the agar surface and incubated at  $35 \pm 2$  °C for 14 hours. Ciprofloxacin (Cipro) (10 ng) and LF-free THDB-crosslinked PVA/bioconjugate films were used as the positive and negative controls, respectively.

## **2.2 Methodologies and principles**

### **2.2.1 SDS-PAGE gel electrophoresis**

SDS-PAGE (sodium dodecyl sulphate polyacrylamide) Gel Electrophoresis is a popular technique for separating proteins according to their molecular weights. The technique begins with denaturation of proteins using SDS, an anionic surfactant that binds to proteins and distributes a homogeneous negative charge proportional to their lengths. The process unfolds proteins, eliminating their native structure and ensuring that the separation is based solely on size, rather than charge or shape. The denatured proteins are subsequently placed in wells of a polyacrylamide gel, which serves as a molecular sieve. When an electric field is applied, negatively charged protein-SDS complexes migrate to the positive electrode. Smaller proteins can move quickly

through the gel, but larger proteins or molecules face more resistance and migrate more slowly. This results in a size-based separation of proteins. After electrophoresis, the gel is stained with dyes like coomassie brilliant blue, which binds to proteins and allows for visualization of the distinct bands representing proteins of different sizes. The distance travelled by each protein band is inversely proportional to its molecular weight. SDS-PAGE is often used to identify proteins, analyze purity, and estimate molecular weight by comparing the migration of sample proteins to a molecular weight marker.

Aliquots of PEG-VEGF<sub>165</sub> bioconjugates were loaded deeply into the wells of a polyacrylamide gel (15%) and subjected to electrophoresis at 200 V for 1 h under non-reducing conditions to characterize bioconjugation. Figure 2.3 shows the lab setup for gel electrophoresis. After electrophoresis, the gel was washed with deionized water three times for 10 min to remove excess SDS. The gel was then stained overnight with Coomassie brilliant blue R-250 dye to visualize bioconjugates. The following day, the gel was washed and destained using a mixture of methanol and acetic acid, to remove excess stain and background. Finally, the gel was analyzed under UV light in a dark room, where bioconjugated protein bands were visualized and analyzed on the basis of molecular weight in comparison to the control or pure VEGF<sub>165</sub>.

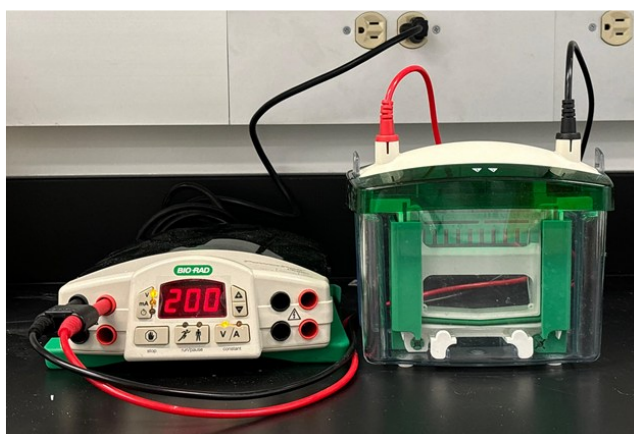


**Figure 2.3** Digital image of a setup for gel electrophoresis.

### 2.2.2 Dynamic light scattering (DLS)

The principle of DLS is based on the measurement of light scattered by particles in a solution undergoing Brownian motion. When a laser light is directed at a sample, the particles scatter the light, and the scattered light fluctuates in intensity over time due to the random motion of the particles. The rate of fluctuation is inversely related to the size of the particles: smaller particles move faster, causing rapid fluctuations, while larger particles move more slowly, resulting in slower fluctuations. By analyzing these fluctuations, DLS calculates the translational diffusion coefficient ( $D$ ) of the particles. The hydrodynamic diameter ( $d(H)$ ) of the particles can then be determined using the Stokes-Einstein equation, which relates diffusion to particle size, solution viscosity, and temperature.

$$d(H) = kT/3\pi\eta D$$

where,  $d(H)$ : hydrodynamic diameter;  $D$ : translational diffusion coefficient;  $K$ : Boltzmann's constant;  $T$ : absolute temperature; and  $\eta$ : viscosity.

### 2.2.3 Circular Dichroism (CD) spectroscopy

CD spectroscopy determines the differential absorption of left- and right-handed circularly polarized light for chiral compounds. When circularly polarized light travels through a chiral sample, the two forms of light are absorbed to varying degrees, resulting in a distinct spectrum. This absorption difference known as circular dichroism, reveals important information about biomolecule's secondary and tertiary structures, such as proteins and nucleic acids. CD is especially effective for investigating protein secondary structures (such as alpha-helices and beta-sheets), tracking protein folding and conformational changes.

Molar ellipticity ( $\Theta$ ) measures the difference in absorption between left- and right-handed circularly polarized light, indicating the degree of circular dichroism. The equation for molar ellipticity is as follows:

$$\Theta = A_{\text{left}} - A_{\text{right}}/c \cdot l$$

where,  $\Theta$ : molar ellipticity (measured in  $\text{deg} \cdot \text{cm}^2 \cdot \text{dmol}^{-1}$ );  $A_{\text{left}}$  and  $A_{\text{right}}$ : absorbances of the left and right circularly polarized light, respectively;  $c$ : concentration of the sample (mol/L); and  $l$ : path length through the sample (cm).

#### **2.2.4 FT-IR spectroscopy**

Fourier Transform Infrared (FT-IR) spectroscopy operates on the absorption of infrared light by a sample, resulting in molecular vibrations in chemical bonds. When infrared radiation flows through a sample, specific wavelengths are absorbed, based on the vibrational frequencies of chemical bonds and functional groups (such as C-H, O-H, and N-H). FT-IR utilizes a Michelson interferometer to gather an interferogram, which is a time-domain signal that represents all light wavelengths at the same time. This signal is then examined using a Fourier transform to provide a frequency-domain spectrum with absorption peaks corresponding to the molecule's vibrational modes. Analyzing these peaks can reveal the sample's chemical makeup, functional groups, and molecular structure.

#### **2.2.5 Disc diffusion method to test antimicrobial properties**

Disc diffusion method, also known as the Kirby-Bauer test, determines the antimicrobial activity of substances against microorganisms. As illustrated in Figure 2.4, a sterile agar plate is first inoculated with a bacterial suspension, ensuring an even spread across the surface. Antibiotic-impregnated sample discs are then placed onto the inoculated agar. The antimicrobial agents in the discs diffuse radially outward, creating a gradient of concentration in the surrounding agar. If the microorganism is susceptible to the antimicrobial agent, it will be inhibited from growing, resulting in a clear zone around the disc, known as the zone of inhibition. The diameter of this inhibition zone is generally measured in millimeters, and larger the zone, the more effective the antimicrobial agent is. The diameter can be measured using a ruler or a caliper, and the results are compared to standardized charts to determine whether the microorganism is susceptible, intermediate, or resistant to the agent. This method provides a qualitative assessment of antimicrobial activity based on the size of the inhibition zones formed.

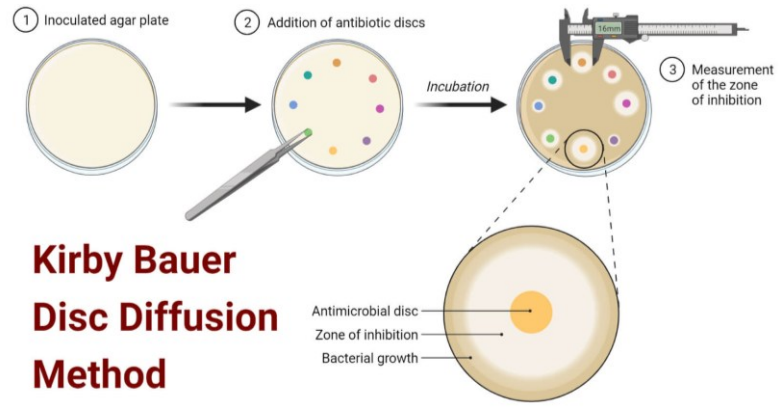


**Figure 2.4** Schematic illustration of Kirby Bauer disc diffusion method for antibiotic susceptibility testing. Copied from Microbe Notes.

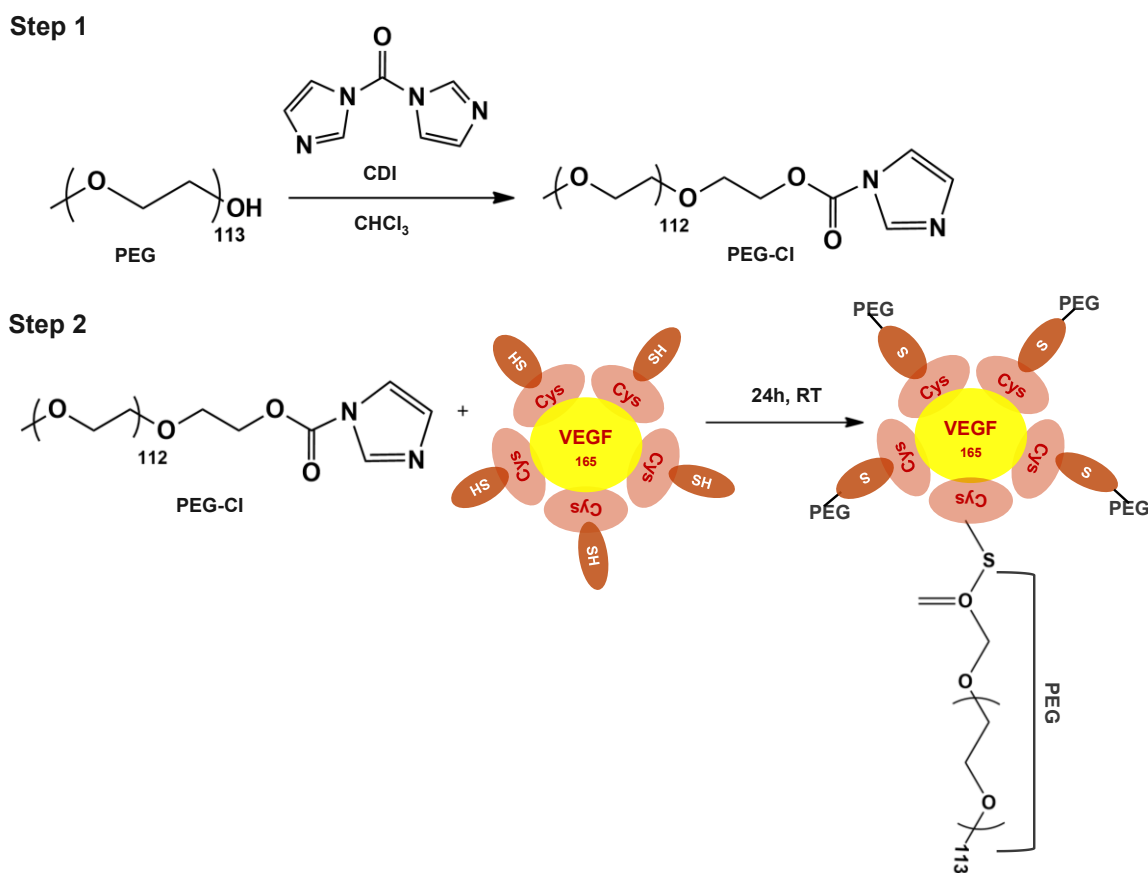
## Result and Discussion

### 3.1 PEGylation of VEGF<sub>165</sub> protein to synthesize PEG-VEGF<sub>165</sub> bioconjugates

Two approaches based on well-known organic, and polymer synthetic methods were explored in this research. They include CDI-mediated and DVS-mediated coupling reactions for PEGylation of VEGF<sub>165</sub>-protein. These approaches involve two steps, with i) the synthesis of reactive PEG precursors as PEG-Cl or PEG-VS and ii) its reaction with pendant thiol groups in cysteine residues in VEGF<sub>165</sub> protein, yielding well-defined PEG-VEGF<sub>165</sub> bioconjugates.

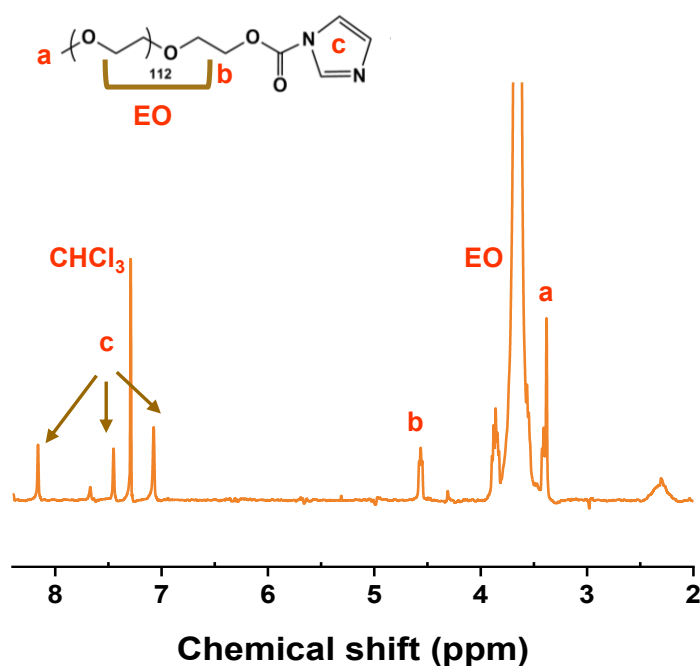
#### 3.1.1 Approach I exploring CDI-mediated coupling reaction

Figure 3.1 illustrates our approach exploring CDI-mediated coupling reaction to synthesize a PEG-VEGF<sub>165</sub> bioconjugate.



**Figure 3.1** Schematic illustration of approach I exploring CDI-mediated coupling reaction to synthesize well-defined PEG-VEGF<sub>165</sub> bioconjugate.

The first step includes PEG activation with CDI to synthesize reactive PEG-CI precursor. CDI-mediated coupling reaction has been used as an effective means to the activation of a terminal hydroxyl group of PEG to synthesize a reactive PEG-CI<sup>149</sup>. In our experiment, PEG reacted with excess CDI as 10/1 mole equivalent ratio of CDI/OH in chloroform at room temperature. The product was purified by precipitation from cold diethyl ether. <sup>1</sup>H NMR spectrum in Figure 3.2 shows the characteristic peak at 4.5 ppm (b) corresponding to methylene protons adjacent to ester bond and peaks at 7.0-8.1 ppm (c) corresponding to imidazole aromatic protons. Their integrals are quantitative to the number of corresponding protons. These results confirm the successful synthesis of PEG-CI.



**Figure 3.2** <sup>1</sup>H NMR spectrum of PEG-CI in CDCl<sub>3</sub>.

The second step involves the reaction of the dried, purified PEG-CI precursor with the thiol groups of cysteine residues of VEGF<sub>165</sub> in aqueous solution. Because VEGF<sub>165</sub> is a water-soluble, engineered macromolecular protein, the characterization of the reaction could not be straightforward. To get an insight into the reaction of the thiol groups of VEGF<sub>165</sub> with the CI group of PEG, a model reaction with DEG-DSH, a small molecular dithiol, was first examined. As depicted in Figure 3.3a, our model reaction includes the reaction of the purified, dried PEG-CI

with DEG-DSH in the presence of DBU as a strong base catalyst in DCM at room temperature. After being purified by cold diethyl ether, the product was characterized by  $^1\text{H}$  NMR analysis. As seen in Figure 3.3b, the new peak at 4.2 ppm (b, c) corresponding to methylene protons adjacent to thiocarbonyl bond appeared, along with the peak at 3.4 ppm corresponding to PEG protons. Their integrals are quantitative to the number of protons, indicating the successful synthesis of PEG-DEG-DS-PEG.

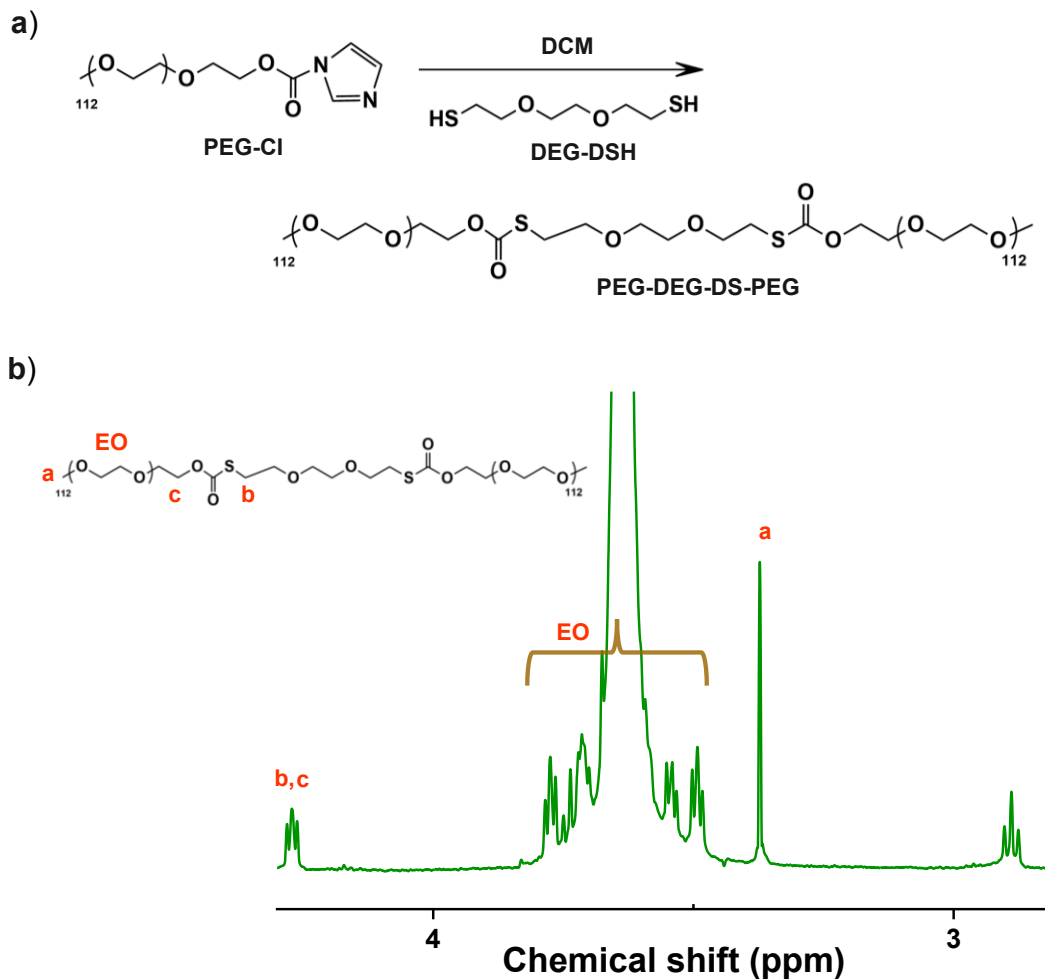


**Figure 3.3** a) Synthetic scheme of model reaction of PEG-Cl with DEG-DSH and b)  $^1\text{H}$  NMR spectrum of PEG-DEG-DS-PEG in  $\text{CDCl}_3$ .

Given our model experiment above, the bioconjugation of PEG with  $\text{VEGF}_{165}$  was studied. As seen in Figure 3.1, the purified dried PEG-Cl precursor (excess) was mixed with an aqueous

VEGF<sub>165</sub> solution. The amount of PEG-CI varied as the wt ratio of PEG-CI/VEGF<sub>165</sub> to be 50/1, 100/1, 200/1, and 300/1. The resulting mixtures, without purification, were characterized by gel electrophoresis, DLS and CD spectroscopy.

Gel electrophoresis results are shown in Figure 3.4. Compared with bare VEGF<sub>165</sub>, all four mixtures stayed at the top of gel because of the bioconjugation of VEGF<sub>165</sub> with PEG to form larger macromolecule PEG-VEGF<sub>165</sub> bioconjugates. This result suggests that all mixtures enabled to form PEG-VEGF bioconjugates, even at PEG/VEGF<sub>165</sub> = 50/1 wt/wt.

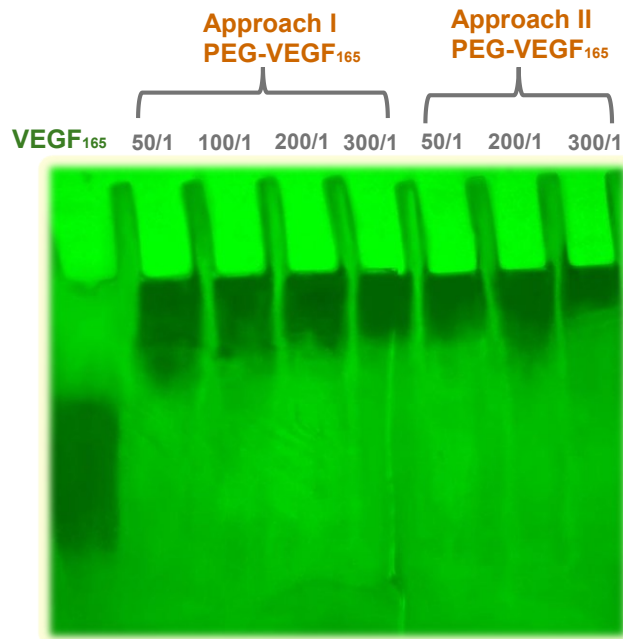


**Figure 3.4** Evaluation of PEG-VEGF<sub>165</sub> bioconjugates prepared at PEG/VEGF<sub>165</sub> = 50/1, 100/1, 200/1, 300/1 wt/wt by native SDS-PAGE gel electrophoresis.

DLS analysis is shown in Figure 3.5. PEG-CI precursor had an average diameter of <10 nm with a monomodal distribution. Promisingly, PEG-VEGF<sub>165</sub> prepared at PEG-VEGF<sub>165</sub> = 300/1 wt/wt had the average diameter significantly increased to >3000 nm.

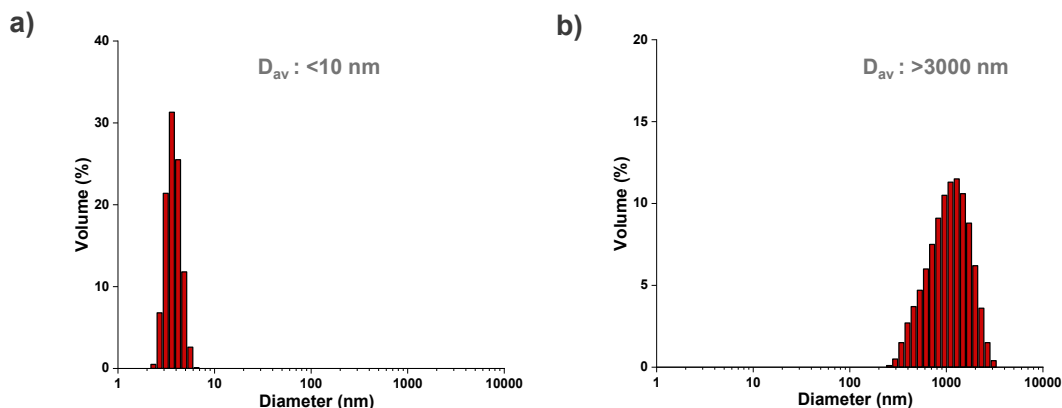


**Figure 3.5** DLS diagrams of (a) PEG-CI and (b) PEG-VEGF<sub>165</sub> bioconjugate prepared via Approach I.

CD spectroscopic analysis to assess the secondary structure of the bioconjugate is shown in Figure 3.6. CD is a powerful technique that measures the differential absorption of left- and right-handed circularly polarized light by chiral molecules, providing insights into the conformational properties of proteins and their interactions with polymers. This technique assesses protein stability and structural changes upon polymer conjugation, revealing the impact of the polymer on the protein's integrity and functionality.

CD in far ultraviolet region (178-260 nm) indicates the secondary structure of protein<sup>150</sup>. BSA protein was chosen as a standard in this experiment (Figure S3.1). As shown in Figure 3.6, the retention of specific spectral regions indicates that certain secondary structure elements of the protein remain unchanged after PEGylation. This suggests that the PEGylation process does not significantly disrupt structural motifs. The stability of the corresponding CD signatures highlights the preservation of key features, such as  $\alpha$ -helices or  $\beta$ -sheets. These findings confirm that PEGylation primarily affects the surface of the protein or other non-structural areas. The overall secondary structure remains largely intact, with minimal perturbation. This supports the conclusion that PEGylation does not cause major conformational changes.

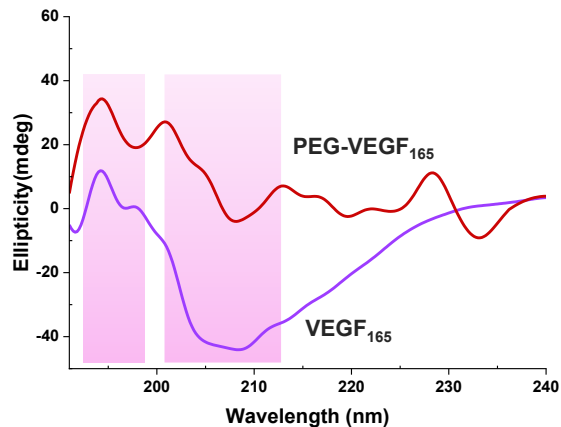


**Figure 3.6** CD spectra of PEG-VEGF<sub>165</sub> bioconjugate (red) prepared using Approach I and bare VEGF<sub>165</sub> protein (purple) for comparison.

### 3.1.2 Approach II exploring DVS-mediated coupling reaction

Figure 3.7 illustrates our approach exploring DVS-mediated coupling reaction to synthesize a PEG-VEGF<sub>165</sub> bioconjugate. This approach has been explored with linear PEG (MW = 6 kg/mol) and 4-arm PEG (MW = 20 kg/mol) for cell-demanded release of VEGF from VEGF-conjugated PEG-peptide hydrogels<sup>151</sup>.

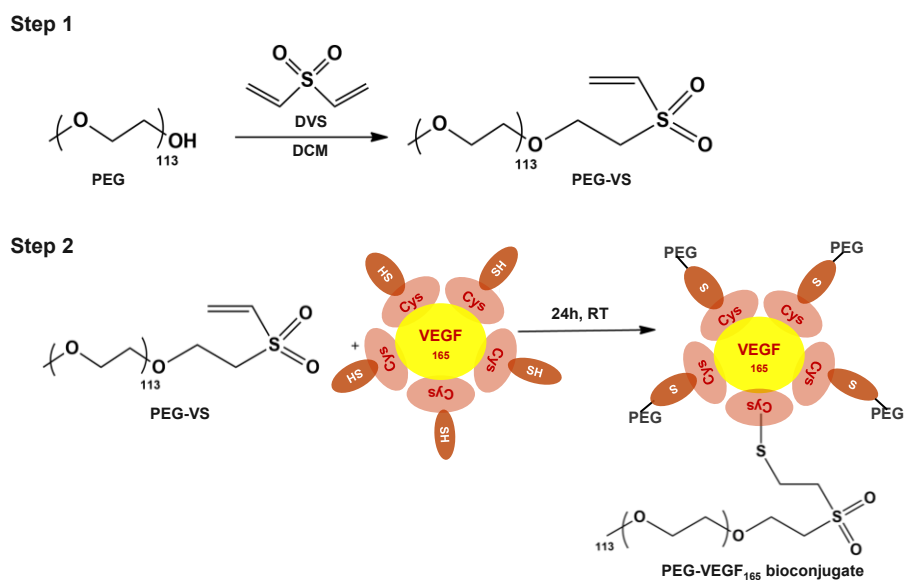


**Figure 3.7** Schematic illustration of approach II exploring DVS-mediated coupling reaction to synthesize well-defined PEG-VEGF<sub>165</sub> bioconjugate.

The first step was the reaction of PEG and DVS at the mole equivalent ratio of DVS/OH = 10/1 in presence of NaH as a base catalyst in DCM at room temperature under inert atmosphere. The product was purified by liquid-liquid extraction, followed by vacuum filtration.  $^1\text{H}$  NMR spectrum in Figure 3.8 shows the characteristics peaks at 6.1-6.8 ppm (b) corresponding to vinyl protons of sulfone moieties and peak at 3.5-4.0 ppm corresponding to PEG protons, suggests the successful synthesis of PEG-VS.

The second step was the reaction of the purified PEG-VS with VEGF<sub>165</sub> in aqueous solution. The amount of PEG-VS varied as wt ratio of PEG-VS/VEGF<sub>165</sub> to be 50/1, 200/1, and 300/1. The resulting mixtures, without purification, were characterized by gel electrophoresis and DLS techniques.

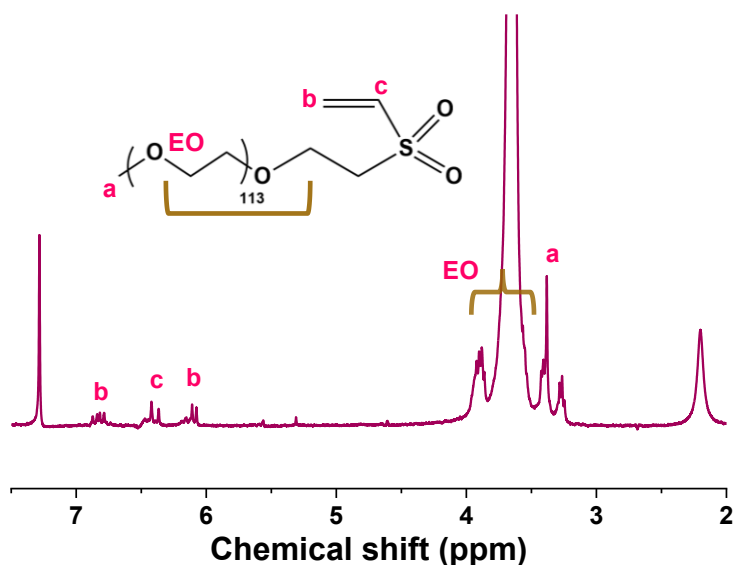


**Figure 3.8**  $^1\text{H}$  NMR spectrum of PEG-VS in  $\text{CDCl}_3$ .

Gel electrophoresis results as shown in Figure 3.4. All three mixtures remained at the top of gel as a consequence of the bioconjugation of VEGF<sub>165</sub> with PEG to form larger macromolecule PEG-VEGF<sub>165</sub> bioconjugates. DLS analysis in Figure 3.9 shows considerable shift in size distribution upon bioconjugation. PEG-VS precursor had an average diameter of 156 nm with bimodal distribution, while PEG bioconjugates prepared at PEG/VEGF<sub>165</sub> = 300/1 wt/wt had the diameter of >1000 nm. These results suggest that DVS chemistry is an efficient means to PEGylation of VEGF proteins, yielding PEG-VEGF<sub>165</sub> bioconjugates.

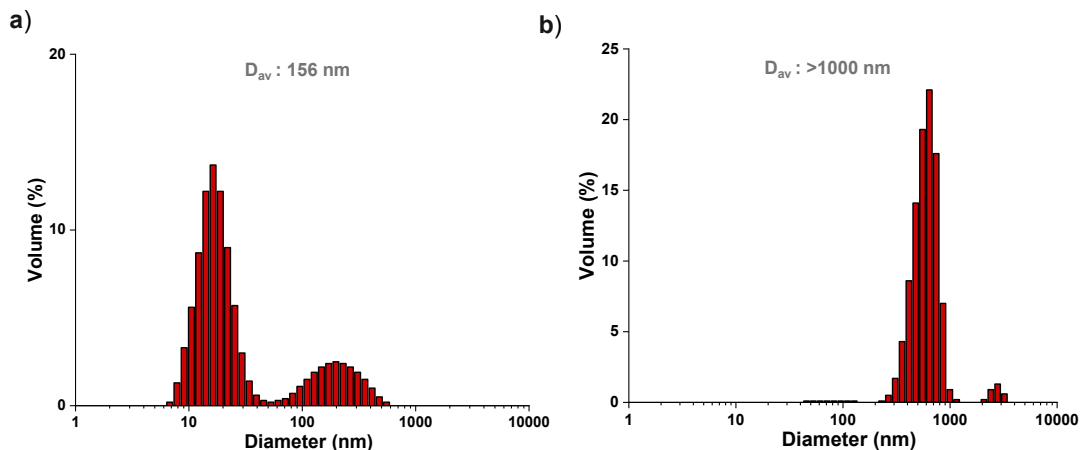


**Figure 3.9** DLS diagrams of (a) PEG-VS and (b) PEG-VEGF<sub>165</sub> bioconjugate prepared using approach II.

### 3.2 Fabrication of BE-crosslinked PVA hydrogels

To fabricate well-defined PVA hydrogel crosslinked through the formation boronic ester bonds between the hydroxyl groups of PVA and boronic acid groups of diboronic acid crosslinkers, (called BE-PVA hydrogels). Two approaches including in-situ crosslinking and post-crosslinking were investigated. Several parameters that could significantly influence were examined, and they include diboronic acids and solvents.

#### 3.2.1 In-situ crosslinking approach

This approach utilizes the direct mixing of aqueous PVA solution with aqueous diboronic acid crosslinker solution in homogeneous medium. The resulting homogenous solutions become viscous, suggesting the occurrence of reaction between OH groups in PVA chains and BA groups of diboronic acid crosslinkers, turning into crosslinked network, as demonstrated in Figure 3.10.

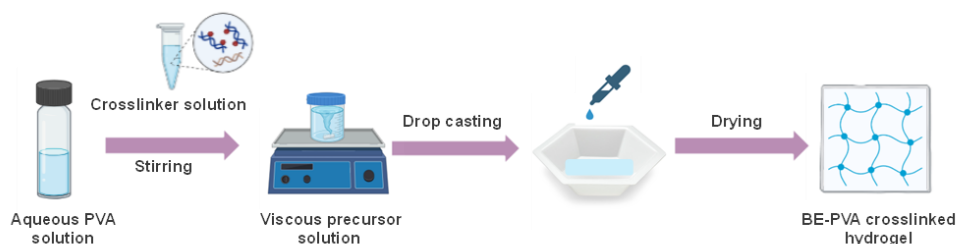


**Figure 3.10** Schematic illustration of in-situ crosslinking approach.

In the first experiment, various diboronic acid crosslinkers were examined, as summarized in Figure 3.11. They include tetrahydroxydiboronic acid (THDB), benzene-1,3-diboronic acid (BDB), and boric acid (BA). They are commercially available and have been used as an effective crosslinker for the fabrication of BE-crosslinked bulk hydrogels without aid of a catalyst at ambient temperature<sup>140, 152, 153</sup>.

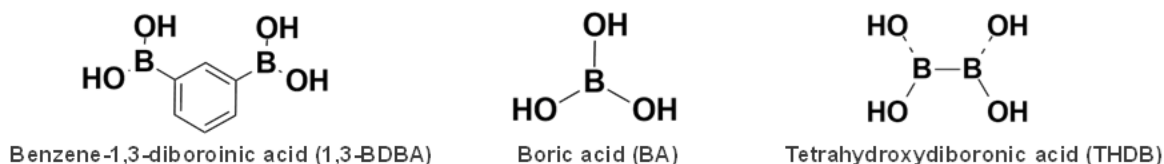


**Figure 3.11** Chemical structure of diboronic acid crosslinkers including BDB, BA and THDB.

First, aliquots of stock solutions of BDB and THDB in DMSO and boric acid in water whose concentrations was 90 mg/mL were mixed with aqueous PVA solutions of 5 and 10% under magnetic stirring. All four formulations were designed with excess diboronic acid crosslinker as mole equivalent ratio of BA/2OH= 2/1. The formed gels were immersed in deionized water for 24 hrs to remove DMSO from gels. Table 3.1 summarizes our results. Wet hydrogels crosslinked with THDB appeared to be dimensionally stable, while those with BDB and boric acid are either fragile or degraded.

**Table 3.1** Characteristics, appearance, and digital images of wet BE-crosslinked PVA hydrogels with water, prepared with diboronic acid crosslinkers including BDB, THDB and boric acid.

| Gels                     | ISC1  | ISC2  | ISC3   | ISC4  |
|--------------------------|---|---|--|---|
| Diboronic acid           | BDB   | boric acid  | THDB   | THDB  |
| Aqueous PVA solution (%) | 10  | 5   | 5  | 10  |
| Apperance of wet gels    | Fragile   | Degraded  | Stable   | Stable  |
| Digital image            |  |  |  |  |

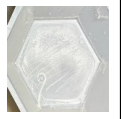
With a choice of THDB as a suitable diboronic acid crosslinker, in the second experiment, the amount of THDB as a mole equivalent ratio of BA/2OH = 0.4/1, 0.6/1, 0.8/1 and 1/1 was investigated for the fabrication of THDB-crosslinked PVA hydrogels (called THBD-PVA). In the experiment, the different volumes of THDB stock solutions in DMSO were mixed with the equal volume of aqueous 5% PVA solution under magnetic stirring. For all four formulations, the increase in viscosity was observed as a result of the occurrence of crosslinking reaction between the hydroxyl group of PVA and the BA groups of THDB. The formed wet gels saturated with DMSO (a high boiling point solvent) were immersed in deionized water for 48 hr to exchange DMSO with water in wet gels. The formed THDB-PVA wet hydrogels were characterized for gel content and swelling ratio in water. As summarized in Table 3.2, all formed THDB-PVA hydrogels had a gel content of 50-53% and swelling ratio of 2.6-3.1. Interestingly, no significant changes were observed with respect to amounts of THDB crosslinker

**Table 3.2** Characteristics, properties, and digital images of THDB-PVA hydrogels.

| Gels            | ISC5  | ISC6  | ISC7   | ISC8  |
|-----------------|---|---|--|---|
| BA/2OH          | 0.4/1   | 0.6/1   | 0.8/1  | 1/1   |
| Gel content (%) | 50  | 52.5  | 51.7   | 50.5  |
| Swelling ratio  | 3.1   | 2.9   | 2.8  | 2.6   |
| Digital image   |  |  |  |  |

In the next experiment, we examined aqueous THBD solution, instead of THBD solution in DMSO for this approach. The reasons include DMSO i) being a high boiling solvent that could not be easy to be removed from hydrogels and ii) denaturing VEGF proteins when being encapsulated, and iii) toxic to skin cells when being used for wound dressing materials. Here, the amounts of PVA and THBD in the mixtures were varied as BA/2OH mole equivalent ratios to be varied at 0.12/1, 0.25/1, 0.03/1 and 0.06/1. The results are summarized in Table 3.3.

**Table 3.3** Characteristics and digital images of THDB-PVA hydrogels prepared with aqueous THBD crosslinker solution.

| Gels                           | ISC-9   | ISC-10  | ISC-11  | ISC-12  | ISC13  | ISC-14  | ISC-15  | ISC-16      |
|--------------------------------|---|---|---|---|--|---|---|-------------|
| Aqueous PVA solution (%)       | 0.5   | 0.5   | 1   | 1   | 2  | 2   | 5   | 5           |
| BA/2OH                         | 0.12/1  | 0.25/1  | 0.12/1  | 0.25/1  | 0.03/1   | 0.06/1  | 0.03/1  | 0.06/1      |
| Apperance of wet gels in water | Flake   | Flake   | Brittle film  | Brittle film  | Film   | Film  | Instant gel   | Instant gel |
| Digital image                  |  |  |  |  |  |  |  |             |

Because of a concern on the possibility of VEGF proteins to be denaturized in the presence of DMSO<sup>154</sup> as a medium for gelation, our choice of the diboronic acid crosslinkers could be limited to THBD which can be dissolved in water. Note that our ultimate goal is the encapsulation of PEG-conjugated VEGF bioconjugate in BE-crosslinked hydrogels. Regardless, there still remain several challenges for the approach with the use of THBD crosslinker. First, THBD has a limited solubility in water (25 mg/mL based on our experiment). Second, the crosslinking reaction between the BA groups of THBD and the OH groups of PVA through the formation of boronic ester (BE) bonds appears to be too fast to control its kinetics. To address these challenges, we have examined the gelation at lower concentration of PVA with less amount of THBD with no stirring. However, our attempts did not appear to be straightforward and to allow the fabrication of THBD-PVA gels in water. Overall, the *in-situ* crosslinking approach did not appear to be a robust means to the fabrication of dimensionally stable BE-crosslinked PVA hydrogels.

### 3.2.2 Post-crosslinking approach

As illustrated in Figure 3.12a, this approach involves two steps, including 1) the fabrication of PVA films in mold and 2) their crosslinked with THDB in water. In the first step aqueous PVA solutions as 5% or 10% was cast in a mold to fabricate PVA films with a defined dimension. After being dried in air, the films were immersed in aqueous THDB solution to induce crosslinking through the formation of boronic ester linkages, as shown in Figure 3.12b.

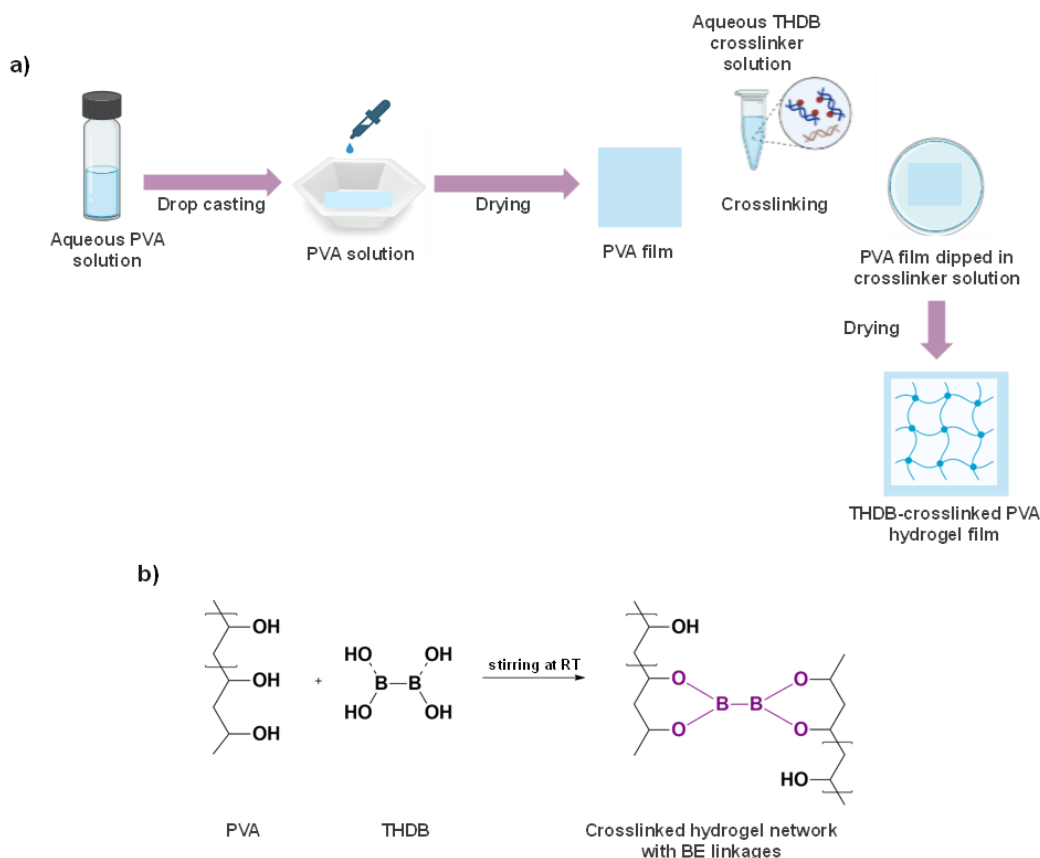


**Figure 3.12** (a) Schematic illustration of post crosslinking approach and (b) crosslinking mechanism by the reaction of PVA with THDB to yield THDB-PVA hydrogel films.

The solubility of THDB in water was examined. The amount of THDB gradually increased in a given volume of water to find out the concentration where excess THDB began to be precipitated from water (not completely dissolved in water). It was found to be 25 mg/mL, which could suggest that the maximum BA/2OH ratio = 4/1 in this approach.

Given knowing the limited solubility of THDB in water, in order to get an insight into how this approach works, we set an experiment where three different sizes of PVA films were cast. The dimensions of these films were PC1 (2.5cm), PC2 (2 cm) and PC3 (1.5 cm) as height, with a consistent width of 1 cm. They were then immersed in an aqueous THDB solution at 25 mg/mL to fabricate THDB-PVA films. Our results are summarized in Table 3.4. Note that mole equivalent ratio of BA/2OH were calculated based on the weight of uncrosslinked PVA films (e.g. mole equivalent of OH groups of PVA in the films). Gel content and swelling ratio were determined in

DMSO which is a good solvent to PVA. Gel content was 51%, 67%, and 87% for PC1, PC2, and PC3 films respectively, suggesting that gel content increased with an increasing size of the films. However, swelling ratios were close to 1.0 for the three films, suggesting no effect of their sizes.

**Table 3.4** Characteristics, properties, and digital images of THDB-PVA hydrogel films prepared by post crosslinking approach.

| Gels                         | Control   | PC1   | PC2  | PC3   |
|------------------------------|---|---|--|---|
| BA/2OH                       | 0   | 0.65/1  | 0.45/1   | 0.13/1  |
| PVA films uncrosslinked (mg) | 97  | 16  | 26   | 81  |
| Gel content (%)              | 0   | 51  | 67   | 87  |
| Swelling ratio               | 0   | 1.01  | 1.08   | 1.04  |
| Digital image                |  |  |  |  |

FT-IR spectroscopic analysis for all three synthesized films (e.g. PC1, PC2 and PC3) was conducted to confirm the formation of BE crosslinks, along with uncrosslinked PVA film as a control. As shown in Figure 3.13, FT-IR spectrum for THDB-PVA films exhibits two characteristic vibrational modes at 1302 and 660  $\text{cm}^{-1}$ , which correspond to B—O—C bending and O—B—O stretching frequencies, respectively<sup>140, 153, 155</sup>. These modes confirm the formation of BE bonds through the reaction of BA groups in THDB with OH groups in PVA, suggesting the fabrication of THDB-PVA hydrogel films. A large vibrational mode at 3320  $\text{cm}^{-1}$  appeared in all FT-IR spectra of three PC1, PC2, and PC3 as well as uncrosslinked PVA, suggesting that a majority of OH groups in PVA remained unreacted with BA groups.

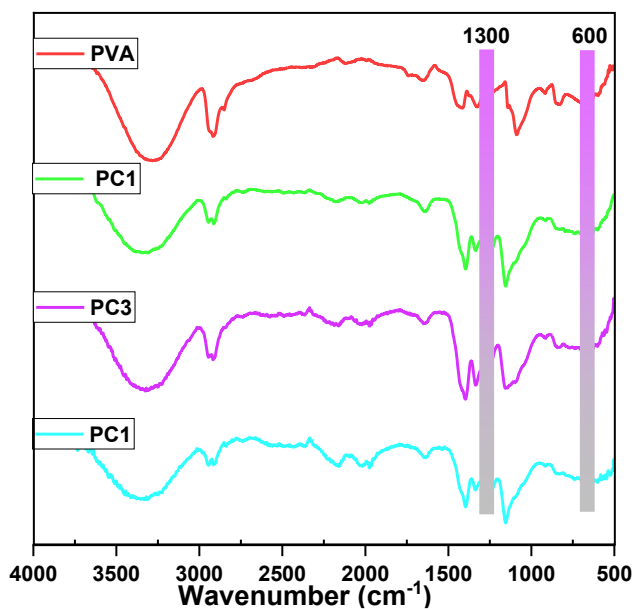


**Figure 3.13** FT-IR spectra of PC-1, 2 and 3 hydrogels films, compared with uncrosslinked PVA as a control.

Uncrosslinked PVA films were tough and not easily dissolved in water. When they were immersed in water for 24 hrs, their insoluble species appeared to be almost negligible, e.g. gel content  $\approx 100\%$  in water. This crosslinking approach involves the immersion of dried PVA films in aqueous THBD solution. Even though the films could be swollen, the access of THBD molecules to OH groups inside PVA films could be limited. It can be imagined that mostly OH groups on the film surfaces could be subjected to the reaction with THBD crosslinkers, resulting in low extent of crosslinking. Interestingly, their gel contents ranged at 50-90% with regard to their sizes. Ultimately, this approach was chosen to fabricate THBD-PVA hydrogels for our further experiments.

### 3.3 Studies of stimuli-responsive degradation (SRD) of THDB-PVA films

Boronic ester bonds are known to respond to stimuli including pHs (both acidic and alkali), hydrogen peroxide, and glucose that can be found in wounds<sup>156</sup>. To investigate the SRD of the fabricated THDB-PVA films, pieces of THDB-PVA films were incubated under conditions described in Section 2.1.7 (Experimental in Chapter 2) and their weight changes were followed for gravimetric analysis to determine their %degradation.

Figure 3.14 shows the results. For pH response shown in Figure 3.14a, %degradation gradually decreased over 6 days of incubation at all pHs, reaching a plateau of approx. 25%. Unexpectedly, no significant difference in %degradation was observed in acidic and alkali pHs, compared with neutral pH. The lack of a significant pH effect may be due to the fact that the majority of the film consists of uncrosslinked PVA, which is not responsive to these pH ranges. In contrast, boronic ester, which could comprise less than 10% of the film, is more pH-sensitive and contributed to 30% degradation of the film. For glucose response shown in Figure 3.14c, % degradation gradually decreased to reach 30% in 6 days. For hydrogen peroxide response shown in Figure 3.14d, %degradation rapidly decreased to 77% in 2 days and gradually decreased to >80% over 6 days. This result suggests the greater impact of hydrogen peroxide as a typical reactive oxygen species found in the wound and body on %degradation of THDB-PVA films. Note that the concentration of hydrogen peroxide in our experiment was 1 M, which is much greater than that (100-200 mM) found in the body.

Overall, pH and glucose had minimal influence on the degradation of THDB-PVA films, while hydrogen peroxide accelerated the degradation of THBD-PVA films. These findings suggest that the synthesized THDB-PVA films are responsive to stimuli (pHs, glucose, and hydrogen peroxide) present in wound environments.

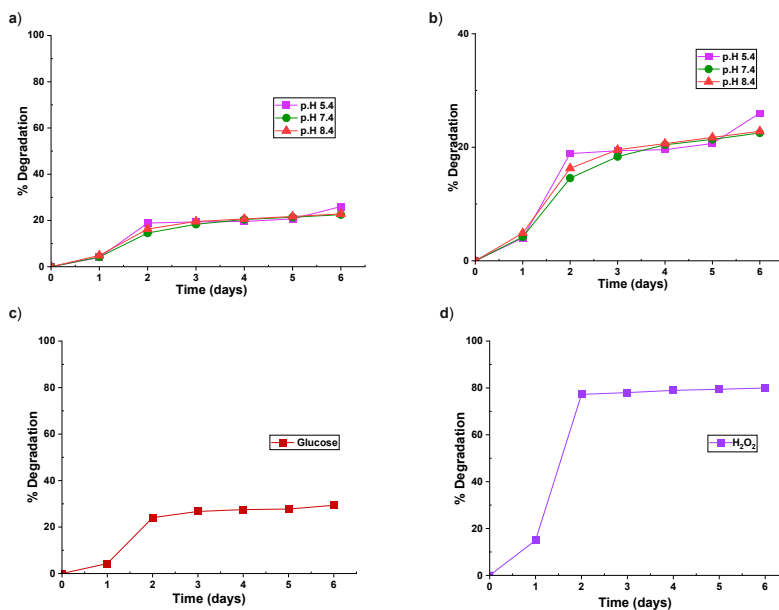


**Figure 3.14** %Degradation of THDB-PVA films in response to (a) pHs, (b) zoomed in version pH's (c) glucose, and (d) hydrogen peroxide.

### 3.4 Encapsulation and location analysis of PEG-VEGF<sub>165</sub> bioconjugates in THDB-PVA films

Post-crosslinking approach was explored to fabricate THDB-PVA films embedded with PEG-VEGF<sub>165</sub> bioconjugates (called THDB-PVA/bioconjugate films). As illustrated in Figure 3.15, a similar procedure was used except for the incorporation of PEG-VEGF<sub>165</sub> prepared at CI/VEGF<sub>165</sub> = 300 w/w in the first step to fabricate PVA films. The formed bioconjugate-loaded PVA films were then immersed in an aqueous THDB solution for BE-induced crosslinking of PVA films.

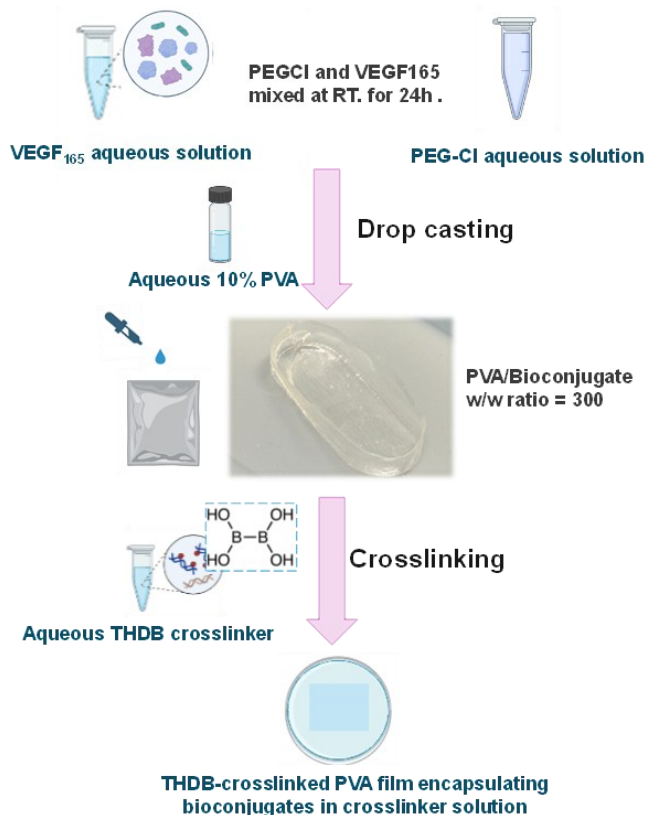


**Figure 3.15** Schematic illustration for the encapsulation of PEG-VEGF<sub>165</sub> bioconjugates in THDB-PVA film to fabricate THBD-PVA/bioconjugate films.

Given the fabrication of THDB-PVA/bioconjugate films, fluorescence microscopy was employed to investigate the location of PEG-VEGF<sub>165</sub> bioconjugates. As illustrated in Figure 3.16, this method utilizes the fluorescent characteristics of fluorescamine dye, which is non-fluorescent, but turns to be fluorescent when it reacts with amino groups in proteins including VEGF<sub>165</sub><sup>157, 158</sup>.

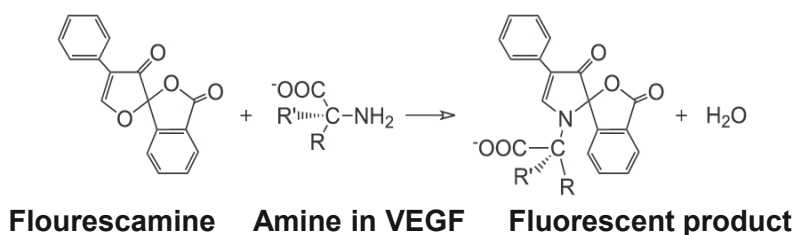


**Figure 3.16** Scheme illustration of the reaction of flourescamine with amine groups in proteins to form fluorescent products for fluorescence microscopy.

In our experiment, films were cut to circular shapes with their diameters to be around 0.8 cm and incubated in aqueous flourescamine solution at room temperature for 2 hrs. Figure 3.17 shows the results. THBD-PVA/VEGF<sub>165</sub> film shows bright fluorescence, but mostly in periphery region (Figure 3.17a). THDB-PVA/bioconjugate film shows fluorescence to some extent (Figure 3.17b). The plausible reason could be PEGylation that could lead to quenching fluorescence as below.

- Steric Hindrance: The large PEG chains can physically block the fluorophore, reducing its ability to emit light<sup>159</sup>.
- Conformational Changes: The attachment of PEG can induce changes in the protein's structure, potentially altering the environment around the fluorophore and affecting its fluorescence properties<sup>160</sup>.
- Microenvironment Alteration: PEGylation can change the local environment around the fluorophore, such as pH or polarity, which can quench fluorescence<sup>161</sup>.

As expected, negative control with no VEGF<sub>165</sub> shows no fluorescence (Figure 3.17c), demonstrating the validity of our experimental protocol.

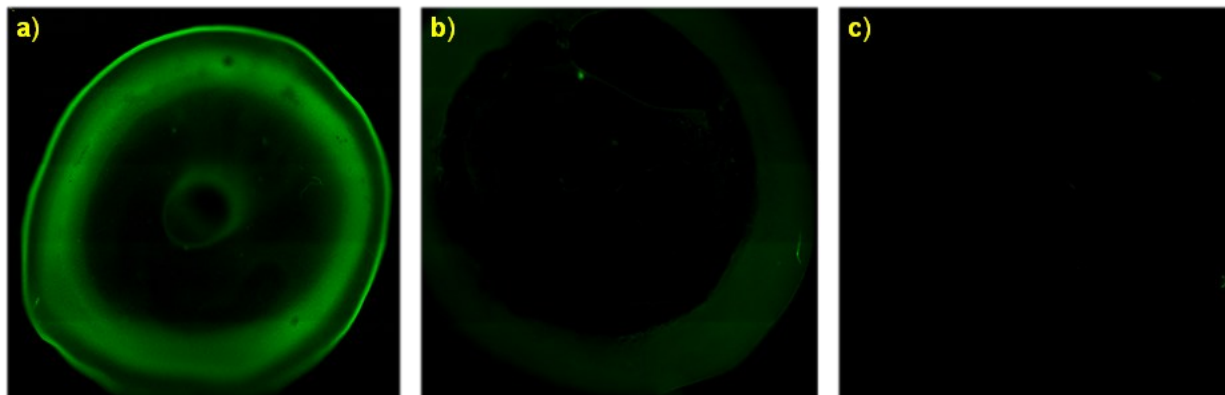


**Figure 3.17** (a) THDB-PVA film encapsulated with VEGF<sub>165</sub>, (a) THDB-PVA/bioconjugate film with (b) and without (c) VEGF<sub>165</sub> as a negative control.

### **3.5 pH responsive release of PEG-VEGF<sub>165</sub> bioconjugates from THDB-PVA/bioconjugate films**

Braford assay, a colorimetric technique used to determine the concentration of proteins, was employed for quantitative analysis of the release of PEG-VEGF<sub>165</sub> bioconjugates from films. This assay relies on binding brilliant blue coomassie dye to proteins. This binding causes a shift in the absorption as absorbance of the dye and the extent of the shift is directly proportional to the concentration of proteins (see Section 2.1.9 in Chapter 2).

First, the correlation curve was constructed with bovine serum albumin (BSA) using UV/vis spectroscopy. A series of aqueous solutions of various concentrations of BSA up to 13  $\mu\text{g/mL}$  were mixed with the given concentration of Coomassie dye and their UV/vis spectra were recorded (Figure S3.2). Then, the absorbance at 595 nm was plotted over the concentration (Figure 3.18).

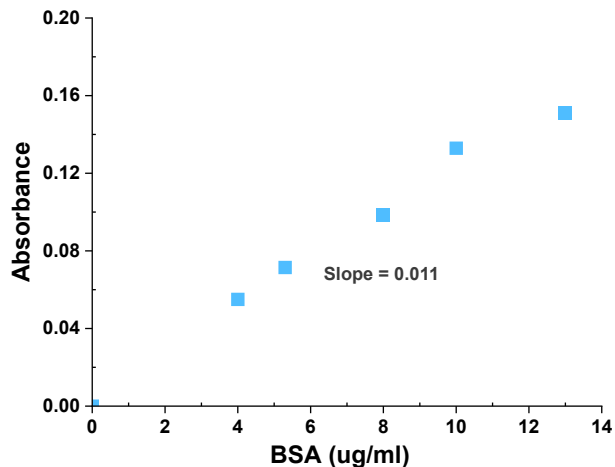


**Figure 3.18** Correlation curve of absorbance at 595 nm over concentration of BSA, a model protein in aqueous solution containing Coomassie dye.

Given the construction of correlation curve of absorbance of BSA as a model protein, pH-responsive release of bioconjugates were conducted. Pieces of the films were incubated at different pHs and their UV/vis spectra mixed with the Bradford reagent were recorded (Figure S3.3). As seen Figure 3.19, the release of bioconjugates increased up to 30% over the incubation time of 4 days at all pHs. As expected from our pH-responsive degradation studies (Section 3.3), no significant difference in %release is observed in both alkali and acidic pHs, compared with neutral pH.

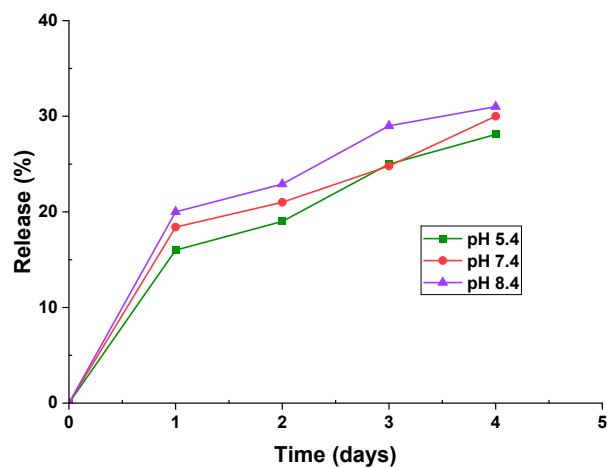


**Figure 3.19** %Release of PEG-VEGF<sub>165</sub> bioconjugates from THDB-PVA/bioconjugate films incubated at different pHs.

### 3.6 Fabrication and antimicrobial properties of LF/THDB-PVA/bioconjugate film

Levofloxacin (LF)-loaded THDB-PVA/bioconjugate film was prepared by post-crosslinking method with a mixture of LF and PVA in 10% aqueous solution. Followed by being cast at room temperature and crosslinked in aqueous THDB solution, the resultant LF/THDB-PVA/bioconjugate films were cut in a circular shape with diameter to be 9 mm.

They were evaluated for antimicrobial properties via a disk diffusion method, in order to forecast their potential for wound dressings. Gram-negative *Escherichia coli* (*E. coli*; ATCC 25922) and the Gram-positive *Staphylococcus aureus* (*S. aureus*; ATCC 29213) were examined. Ciprofloxacin (10 µg) as a positive control and pieces of paper as a negative control were included in our experiment. All tested samples were intended to contain the same amount of LF.

Figure 3.20 shows the results with the diameter of inhibition (DOI) and digital images. Note that larger DOI values suggest greater antimicrobial activity. It was interesting that the antimicrobial activity of the developed films appeared to be greater against *E. coli*, compared with *S. aureus*. This could be attributed to different susceptibilities of those bacteria to antibiotics.

Compared with the DOI of 3.8 for the ciprofloxacin drug, the DOI was 3 for crosslinked film and 5 for an uncrosslinked film against *E. coli*. A similar trend was observed with a DOI of 2.8 for crosslinked films and 4.1 for uncrosslinked for uncrosslinked films against *S. aureus*. Both results confirm that uncrosslinked films had greater antimicrobial properties than crosslinked mats, this is plausibly due to incomplete release of LF in crosslinked films. Interestingly uncrosslinked films had greater antimicrobial properties than the ciprofloxacin drug itself.

The THDB-PVA/bioconjugate film without LF, with or without crosslinking exhibited a DOI of 2. Overall, the THDB-PVA/bioconjugate film demonstrated a good DOI even in the absence of LF, indicating that the film itself possesses antimicrobial properties.

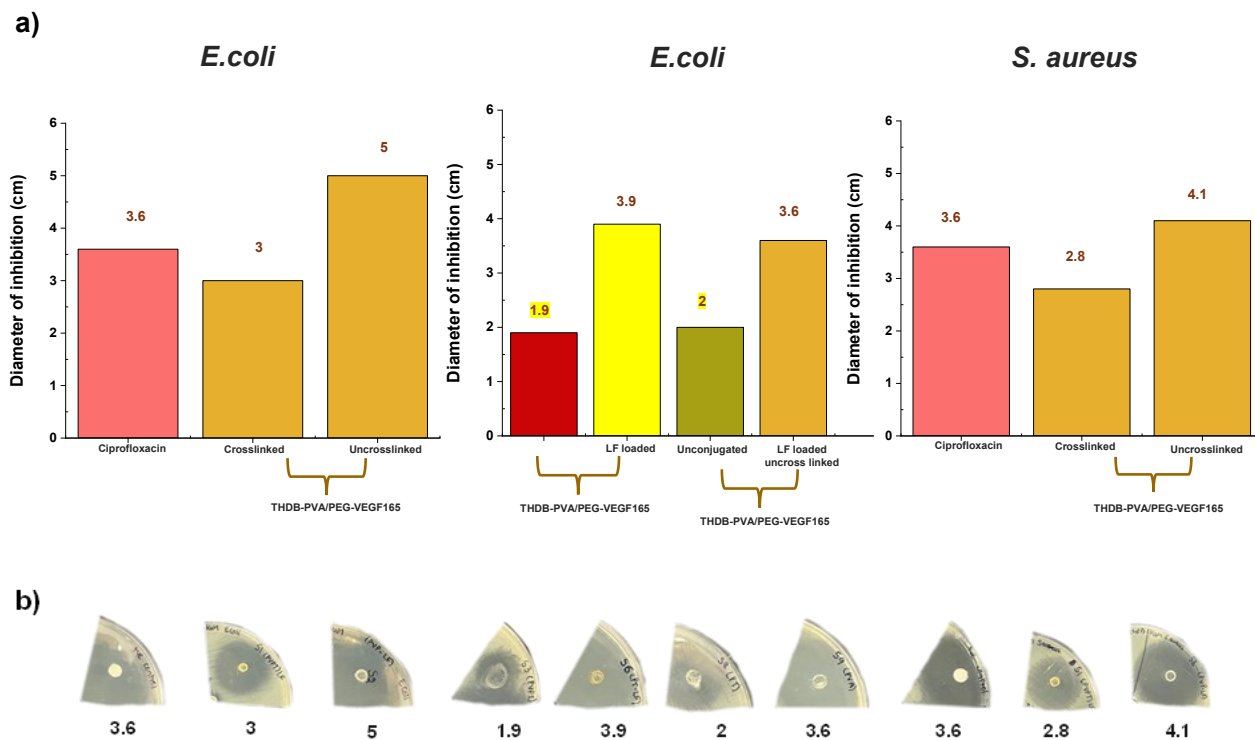


**Figure 3.20** a) DOI and b) digital images of Ciprofloxacin itself, crosslinked and uncrosslinked LF/THDB-PVA/bioconjugate films over Gram-negative *E. coli* and Gram-positive *S. aureus*.

### 3.7 Supplementary Figures for Chapter 3

**Figure S3.1** CD spectra of BSA model protein.

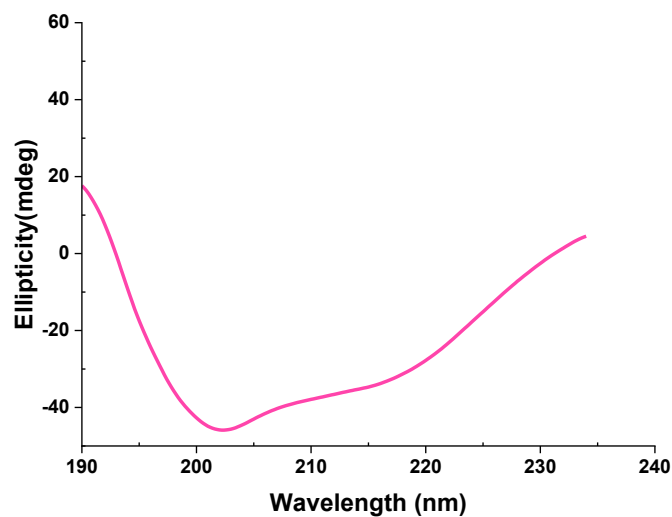


**Figure S3.2** Overlaid UV-vis spectra of aqueous solutions of various concentrations up to 13  $\mu\text{g/mL}$  containing Bradford reagent.

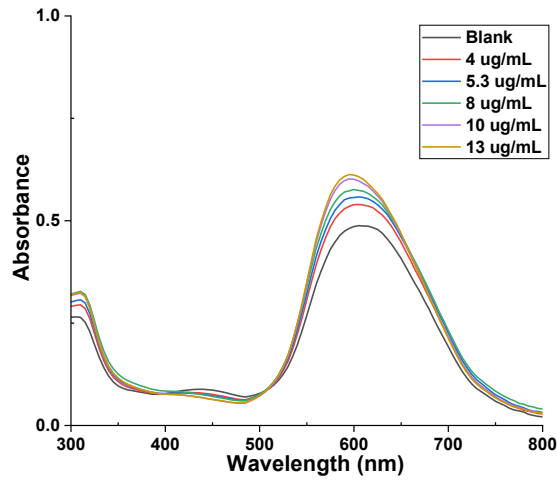
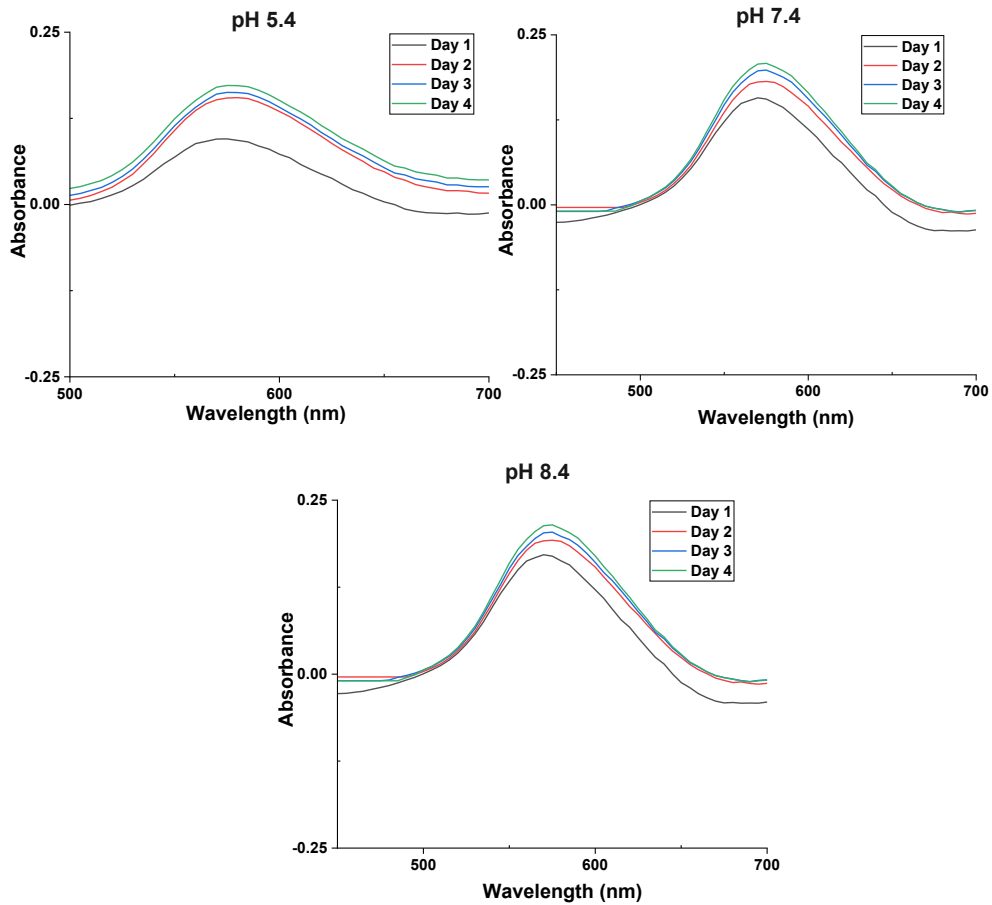


**Fig S3.3** Overlaid UV-Vis spectrums illustrating the % release of bioconjugates from incubated pieces of THDB-PVA/bioconjugate films at different pH values (5.4, 7.4, and 8.4).



## Conclusion and future work

### 4.1 Conclusion

My MSc research developed an effective pH-responsive degradable hydrogel film encapsulating PEG-VEGF<sub>165</sub> bioconjugates, potentially exhibiting cell proliferation and angiogenesis at the injury site, to accelerate the healing process in chronic wounds.

Chapter 2 describes experiments and methods to explore the applications of polymer-protein bioconjugates in THDB-crosslinked PVA hydrogel films. To synthesize the bioconjugates, two well-known approaches, named CDI and DVS-mediated coupling chemistries, were utilized, and the bioconjugates were characterized using various analytical techniques, including CD spectroscopy, to ensure the integrity of VEGF protein structure during PEGylation. The fabrication of PVA hydrogel films, followed by their crosslinking with THDB diboronic acid crosslinker ensured their structural integrity and the incorporation of bioconjugates into hydrogel film. Fluorescence microscopy was utilized to determine the presence and location of bioconjugates in hydrogel films. A key experiment focused on stimuli-responsive degradation of THDB-crosslinked hydrogel films encapsulating bioconjugates in a wound environment (pH, glucose and ROS). Further, Bradford assay was employed to study the release of bioconjugates from hydrogel films in response to change in pH, mimicking wound environments. The encapsulation of LF in THDB-PVA/bioconjugate films was also investigated, with subsequent antimicrobial studies to assess the efficacy.

Chapter 3 describes our results that are summarized with positive outcomes. The successful synthesis of bioconjugates was confirmed through SDS-PAGE gel electrophoresis and further validated by DLS analysis. The fabrication of THDB-crosslinked PVA hydrogel films was achieved using a post-crosslinking approach, followed by characterization with FT-IR spectroscopy to confirm the formation of boronate ester linkages. PEG-VEGF<sub>165</sub> bioconjugates were incorporated into the films and tested for stimuli responsiveness in a wound environment. It was observed that the THDB-PVA/bioconjugate films released approximately 30% of the bioconjugates over 4 days, closely matching the degradation rate of the film. Finally, LF was

loaded into the hydrogel films, and its antimicrobial efficacy was evaluated using the disc diffusion method.

Overall, the developed LF-loaded THDB-PVA/bioconjugate film, with response to wound pH, glucose, and ROS, demonstrates a robust approach for designing a dermal wound healing system. This system targets the healing window by incorporating angiogenic VEGF<sub>165</sub>, exhibiting an enhanced and accelerated release of encapsulated bioconjugates at the injury site.

#### **4.2 Future work**

Future directions for this project will focus on advancing both *in vitro* and *in vivo* tests to assess the potential of LF-loaded THDB-PVA/bioconjugate films in wound healing applications.

*In vitro* tests will explore the biocompatibility, cytotoxicity, and ability of hydrogel films to support cell behavior, using various cell types such as fibroblasts, keratinocytes, and endothelial cells. This will include evaluating cell proliferation, migration, and the interaction with the bioconjugates, as well as investigating the controlled release of bioconjugates in these models. These studies will provide insights into how the films promote healing at the cellular level and refine their design for clinical use.

*In vivo* tests (animal models) will evaluate the real-world performance of the developed hydrogel films under physiological conditions. *In vivo* studies will assess how well the films promote tissue regeneration, angiogenesis, and antimicrobial activity at the wound site. Tests will also confirm the films' degradation rate, release profiles, and their ability to provide sustained release of bioconjugates over time, offering crucial data on their therapeutic efficacy and overall interaction with the biological environment.

## References

1. S. Dhivya, V. V. Padma and E. Santhini, *Biomedicine (Taipei)*, 2015, 5, 22.
2. M. C. Robson, *Curr Problems Surg*, 2001, 38, 61-140.
3. M. Szycher and S. J. Lee, *Journal of biomaterials applications*, 1992, 7, 142-213.
4. S. Schreml, R. Szeimies, L. Prantl, S. Karrer, M. Landthaler and P. Babilas, *British Journal of Dermatology*, 2010, 163, 257-268.
5. G. S. Lazarus, D. M. Cooper, D. R. Knighton, D. J. Margolis, R. E. Percoraro, G. Rodeheaver and M. C. Robson, *Wound repair and regeneration*, 1994, 2, 165-170.
6. B. A. Mast and G. S. Schultz, *Wound Repair and Regeneration*, 1996, 4, 411-420.
7. F. Strodbeck, *Newborn and infant nursing reviews*, 2001, 1, 43-52.
8. G. Hosgood, *Veterinary Clinics: Small Animal Practice*, 2006, 36, 667-685.
9. G. K. Srivastava, S. Martinez-Rodriguez, N. I. Md Fadilah, D. Looi Qi Hao, G. Markey, P. Shukla, M. B. Fauzi and F. Panetsos, *Polymers*, 2024, 16, 1280.
10. C. Daunton, S. Kothari, L. Smith and D. Steele, *J. Aust. Wound Manage. Assoc*, 2012, 20, 174.
11. S. Dhivya, V. V. Padma and E. Santhini, *BioMedicine*, 2015, 5, 22.
12. J. S. Boateng, K. H. Matthews, H. N. Stevens and G. M. Eccleston, *Journal of pharmaceutical sciences*, 2008, 97, 2892-2923.
13. J. B. Shah, *J Am Col Certif Wound Spec*, 2011, 3, 65-66.
14. D. Queen, H. Orsted, H. Sanada and G. Sussman, *International wound journal*, 2004, 1, 59-77.
15. L. Diaz-Gomez, I. Gonzalez-Prada, R. Millan, A. Da Silva-Candal, A. Bugallo-Casal, F. Campos, A. Concheiro and C. Alvarez-Lorenzo, *Carbohydrate Polymers*, 2022, 278, 118924.
16. S. Thomas, *Journal of wound care*, 2000, 9, 56-60.
17. S. Ahmed and S. Ikram, *Achievements in the Life Sciences*, 2016, 10, 27-37.
18. S. Gajbhiye and S. Wairkar, *Biomaterials Advances*, 2022, 142, 213152.
19. R. D. Price, S. Myers, I. M. Leigh and H. A. Navsaria, *American journal of clinical dermatology*, 2005, 6, 393-402.
20. S. Prete, M. Dattilo, F. Patitucci, G. Pezzi, O. I. Parisi and F. Puoci, *Journal of Functional Biomaterials*, 2023, 14, 455.
21. J.-O. Jeong, J.-S. Park, E. J. Kim, S.-I. Jeong, J. Y. Lee and Y.-M. Lim, *International Journal of Molecular Sciences*, 2020, 21, 187.
22. V. Tangpasuthadol, N. Pongchaisirikul and V. P. Hoven, *Carbohydr Res*, 2003, 338, 937-942.
23. L. Y. Qiu and Y. H. Bae, *Pharmaceutical Research*, 2006, 23, 1-30.
24. D. F. Williams, *Bioactive Materials*, 2022, 10, 306-322.
25. Y.-J. Lin, G.-H. Lee, C.-W. Chou, Y.-P. Chen, T.-H. Wu and H.-R. Lin, *Journal of Materials Chemistry B*, 2015, 3, 1931-1941.
26. B. Schmidt, *Journal*, 2006.
27. S. Ricard-Blum, *Cold Spring Harbor perspectives in biology*, 2011, 3, a004978.
28. L. Harsha and M. Brundha, *Drug Invention Today*, 2020, 13.
29. J. Slavin, *J Pathol*, 1996, 178, 5-10.
30. J. W. Weisel, in *Advances in Protein Chemistry*, Academic Press, 2005, vol. 70, pp. 247-299.

31. P. Heher, S. Mühleder, R. Mittermayr, H. Redl and P. Slezak, *Advanced Drug Delivery Reviews*, 2018, 129, 134-147.
32. G. C. Gurtner, S. Werner, Y. Barrandon and M. T. Longaker, *Nature*, 2008, 453, 314-321.
33. L. Vaidyanathan, *Biomed Pharmacol J*, 2021, 14, 1469-1480.
34. P. Bao, A. Kodra, M. Tomic-Canic, M. S. Golinko, H. P. Ehrlich and H. Brem, *Journal of Surgical Research*, 2009, 153, 347-358.
35. M. G. Tonnesen, X. Feng and R. A. Clark, 2000.
36. R. Roskoski, *Critical Reviews in Oncology/Hematology*, 2007, 62, 179-213.
37. A. Witmer, G. Vrensen, C. Van Noorden and R. Schlingemann, *Progress in retinal and eye research*, 2003, 22, 1-29.
38. R. Roskoski Jr, *Pharmacological Research*, 2017, 120, 116-132.
39. A. Mohandas, B. Anisha, K. Chennazhi and R. Jayakumar, *Colloids and Surfaces B: Biointerfaces*, 2015, 127, 105-113.
40. P. Losi, E. Briganti, C. Errico, A. Lisella, E. Sanguinetti, F. Chiellini and G. Soldani, *Acta biomaterialia*, 2013, 9, 7814-7821.
41. H. L. Xu, W. Z. Yu, C. T. Lu, X. K. Li and Y. Z. Zhao, *Biotechnology Journal*, 2017, 12, 1600243.
42. F.-M. Chen, Y. An, R. Zhang and M. Zhang, *Journal of controlled release*, 2011, 149, 92-110.
43. I. Freeman and S. Cohen, *Biomaterials*, 2009, 30, 2122-2131.
44. J. Ziegler, D. Anger, F. Krummenauer, D. Breitig, S. Fickert and K. P. Guenther, *Journal of Biomedical Materials Research Part A: An Official Journal of The Society for Biomaterials, The Japanese Society for Biomaterials, and The Australian Society for Biomaterials and the Korean Society for Biomaterials*, 2008, 86, 89-97.
45. M. M. Martino, P. S. Briquez, K. Maruyama and J. A. Hubbell, *Advanced drug delivery reviews*, 2015, 94, 41-52.
46. I. Capila and R. J. Linhardt, *Angewandte Chemie International Edition*, 2002, 41, 390-412.
47. A. K. Jha, A. Mathur, F. L. Svedlund, J. Ye, Y. Yeghiazarians and K. E. Healy, *Journal of Controlled Release*, 2015, 209, 308-316.
48. Y. Tabata, *Journal of the Royal Society interface*, 2009, 6, S311-S324.
49. D. Enriquez-Ochoa, P. Robles-Ovalle, K. Mayolo-Deloisa and M. E. G. Brunck, *Front Bioeng Biotechnol*, 2020, 8, 620.
50. K. S. Masters, *Macromolecular bioscience*, 2011, 11, 1149-1163.
51. Z. Wang, Z. Wang, W. W. Lu, W. Zhen, D. Yang and S. Peng, *NPG Asia Materials*, 2017, 9, e435-e435.
52. G. Francis, D. Fisher, C. Delgado, F. Malik, A. Gardiner and D. Neale, *International journal of hematology*, 1998, 68, 1-18.
53. J. D. Wallat, K. A. Rose and J. K. Pokorski, *Polym. Chem.*, 2014, 5, 1545-1558.
54. Y. Wu, D. Y. W. Ng, S. L. Kuan and T. Weil, *Biomaterials Science*, 2015, 3, 214-230.
55. H. Schlaad and N. R. Cameron, *Bio-synthetic polymer conjugates*, Springer-Verlag, Heidelberg ;, 2013.
56. J. P. Magnusson, S. Bersani, S. Salmaso, C. Alexander and P. Caliceti, *Bioconjugate Chemistry*, 2010, 21, 671-678.
57. S. Averick, A. Simakova, S. Park, D. Konkolewicz, A. J. D. Magenau, R. A. Mehl and K. Matyjaszewski, *ACS Macro Letters*, 2012, 1, 6-10.
58. W. Zhao, F. Liu, Y. Chen, J. Bai and W. Gao, *Polymer*, 2015, 66, A1-A10.

59. L. A. Canalle, D. W. Löwik and J. C. van Hest, *Chemical Society Reviews*, 2010, 39, 329-353.
60. H. Schlaad, *Bio-synthetic polymer conjugates*, Springer, 2012.
61. J. C. Foster, S. Varlas, B. Couturaud, Z. Coe and R. K. O'Reilly, *Journal of the American Chemical Society*, 2019, 141, 2742-2753.
62. S. Gundecha, S. Shirolkar, S. Deshkar, S. Chitlange, S. Shewale and R. A. Jagtap, *International Journal of Health Sciences*, 2022, 6622-6634.
63. S. Jevševar, M. Kunstelj and V. G. Porekar, *Biotechnology Journal: Healthcare Nutrition Technology*, 2010, 5, 113-128.
64. C. Li, T. Li, X. Tian, W. An, Z. Wang, B. Han, H. Tao, J. Wang and X. Wang, *Frontiers in Pharmacology*, 2024, 15, 1353626.
65. S. Salmaso and P. Caliceti, in *Peptide and protein delivery*, Elsevier, 2011, pp. 247-290.
66. M. Roberts, M. Bentley and J. Harris, *Advanced drug delivery reviews*, 2002, 54, 459-476.
67. S. Herman, G. Hooftman and E. Schacht, *Journal of bioactive and compatible polymers*, 1995, 10, 145-187.
68. S. L. Ho and A. H.-J. Wang, *Journal of the Taiwan Institute of Chemical Engineers*, 2009, 40, 123-129.
69. C. Zhang, X.-l. Yang, Y.-h. Yuan, J. Pu and F. Liao, *BioDrugs*, 2012, 26, 209-215.
70. A. Rondon, S. Mahri, F. Morales-Yanez, M. Dumoulin and R. Vanbever, *Advanced Functional Materials*, 2021, 31, 2101633.
71. A. Lee and L. J. Scott, *BioDrugs*, 2020, 34, 235-244.
72. O. Luneva, R. Olekhovich and M. Uspenskaya, *Polymers*, 2022, 14, 3135.
73. P. Korla, *BioDrugs*, 2012, 26, 163-175.
74. K. Katoh, T. Tanabe and K. Yamauchi, *Biomaterials*, 2004, 25, 4255-4262.
75. G. Ramanathan, S. Singaravelu, T. Muthukumar, S. Thyagarajan, P. T. Perumal and U. T. Sivagnanam, *Materials Science and Engineering: C*, 2017, 72, 359-370.
76. P. Chandika, S.-C. Ko, G.-W. Oh, S.-Y. Heo, V.-T. Nguyen, Y.-J. Jeon, B. Lee, C. H. Jang, G. Kim, W. S. Park, W. Chang, I.-W. Choi and W.-K. Jung, *International Journal of Biological Macromolecules*, 2015, 81, 504-513.
77. W. Wang, S. Lin, Y. Xiao, Y. Huang, Y. Tan, L. Cai and X. Li, *Life Sciences*, 2008, 82, 190-204.
78. C. Jinno, N. Morimoto, R. Ito, M. Sakamoto, S. Ogino, T. Taira and S. Suzuki, *BioMed research international*, 2016, 2016, 4567146.
79. A. R. Chandrasekaran, J. Venugopal, S. Sundarrajan and S. Ramakrishna, *Biomedical Materials*, 2011, 6, 015001.
80. A. Tamayol, M. Akbari, N. Annabi, A. Paul, A. Khademhosseini and D. Juncker, *Biotechnology Advances*, 2013, 31, 669-687.
81. W. J. Li, C. T. Laurencin, E. J. Caterson, R. S. Tuan and F. K. Ko, *Journal of Biomedical Materials Research: An Official Journal of The Society for Biomaterials, The Japanese Society for Biomaterials, and The Australian Society for Biomaterials and the Korean Society for Biomaterials*, 2002, 60, 613-621.
82. M. Wang, A. K. Roy and T. J. Webster, *Frontiers in physiology*, 2017, 7, 683.
83. G. C. Ingavle and J. K. Leach, *Tissue Engineering Part B: Reviews*, 2014, 20, 277-293.
84. K. S. Rho, L. Jeong, G. Lee, B.-M. Seo, Y. J. Park, S.-D. Hong, S. Roh, J. J. Cho, W. H. Park and B.-M. Min, *Biomaterials*, 2006, 27, 1452-1461.

85. M. S. Khil, D. I. Cha, H. Y. Kim, I. S. Kim and N. Bhattarai, *Journal of Biomedical Materials Research Part B: Applied Biomaterials: An Official Journal of The Society for Biomaterials, The Japanese Society for Biomaterials, and The Australian Society for Biomaterials and the Korean Society for Biomaterials*, 2003, 67, 675-679.
86. X. Sun, Q. Lang, H. Zhang, L. Cheng, Y. Zhang, G. Pan, X. Zhao, H. Yang, Y. Zhang and H. A. Santos, *Advanced Functional Materials*, 2017, 27, 1604617.
87. R. A. Thakur, C. A. Florek, J. Kohn and B. B. Michniak, *International Journal of Pharmaceutics*, 2008, 364, 87-93.
88. A. R. Sadeghi-Avalshahr, M. Khorsand-Ghayeni, S. Nokhasteh, A. M. Molavi and H. Naderi-Meshkin, *Journal of Materials Science: Materials in Medicine*, 2017, 28, 14.
89. V. T. Tchemtchoua, G. Atanasova, A. Aqil, P. Filée, N. Garbacki, O. Vanhooteghem, C. Deroanne, A. Noël, C. Jérôme, B. Nusgens, Y. Poumay and A. Colige, *Biomacromolecules*, 2011, 12, 3194-3204.
90. B. Veleirinho, D. S. Coelho, P. F. Dias, M. Maraschin, R. M. Ribeiro-do-Valle and J. A. Lopes-da-Silva, *International Journal of Biological Macromolecules*, 2012, 51, 343-350.
91. S. Zhang, C. Vlémincq, D. R. Wong, D. Magnin, K. Glinel, S. Demoustier-Champagne and A. M. Jonas, *Journal of Materials Chemistry B*, 2016, 4, 7651-7661.
92. J. S. Choi, K. W. Leong and H. S. Yoo, *Biomaterials*, 2008, 29, 587-596.
93. B. J. Kim, H. Cheong, E. S. Choi, S. H. Yun, B. H. Choi, K. S. Park, I. S. Kim, D. H. Park and H. J. Cha, *Journal of Biomedical Materials Research Part A*, 2017, 105, 218-225.
94. J. L. Lowery, N. Datta and G. C. Rutledge, *Biomaterials*, 2010, 31, 491-504.
95. J. S. Boateng, K. H. Matthews, H. N. E. Stevens and G. M. Eccleston, *Journal of Pharmaceutical Sciences*, 2008, 97, 2892-2923.
96. S. P. Miguel, M. P. Ribeiro, H. Brancal, P. Coutinho and I. J. Correia, *Carbohydrate Polymers*, 2014, 111, 366-373.
97. J. L. Drury and D. J. Mooney, *Biomaterials*, 2003, 24, 4337-4351.
98. A. Tamayol, A. H. Najafabadi, B. Aliakbarian, E. Arab-Tehrany, M. Akbari, N. Annabi, D. Juncker and A. Khademhosseini, *Advanced healthcare materials*, 2015, 4, 2146-2153.
99. J. O. Kim, J. K. Park, J. H. Kim, S. G. Jin, C. S. Yong, D. X. Li, J. Y. Choi, J. S. Woo, B. K. Yoo, W. S. Lyoo, J.-A. Kim and H.-G. Choi, *International Journal of Pharmaceutics*, 2008, 359, 79-86.
100. E. Chung, V. Y. Rybalko, P. L. Hsieh, S. L. Leal, M. A. Samano, A. N. Willauer, R. S. Stowers, S. Natesan, D. O. Zamora and R. J. Christy, *Wound Repair and Regeneration*, 2016, 24, 810-819.
101. A. Assmann, A. Vegh, M. Ghasemi-Rad, S. Bagherifard, G. Cheng, E. S. Sani, G. U. Ruiz-Esparza, I. Noshadi, A. D. Lassaletta, S. Gangadharan, A. Tamayol, A. Khademhosseini and N. Annabi, *Biomaterials*, 2017, 140, 115-127.
102. N. Annabi, Y.-N. Zhang, A. Assmann, E. S. Sani, G. Cheng, A. D. Lassaletta, A. Vegh, B. Dehghani, G. U. Ruiz-Esparza and X. Wang, *Science translational medicine*, 2017, 9, eaai7466.
103. O. Wichterle and D. Lim, *Nature*, 1960, 185, 117-118.
104. A. Heenan, *J Wound Care*, 1999, 8, 69-72.
105. J. Debra and O. Cheri, *Technology Catalysts International Corporation*, 1998, 2, 1-185.
106. H. Liu, Y. Wang, K. Cui, Y. Guo, X. Zhang and J. Qin, *Advanced Materials*, 2019, 31, 1902042.

107. D. A. Gyles, L. D. Castro, J. O. C. Silva Jr and R. M. Ribeiro-Costa, *European Polymer Journal*, 2017, 88, 373-392.
108. X. Liang, C. Huang, H. Liu, H. Chen, J. Shou, H. Cheng and G. Liu, *Chinese Chemical Letters*, 2024, 35, 109442.
109. P. A. Janmey, J. P. Winer and J. W. Weisel, *Journal of the Royal Society Interface*, 2009, 6, 1-10.
110. G. Sun, X. Zhang, Y.-I. Shen, R. Sebastian, L. E. Dickinson, K. Fox-Talbot, M. Reinblatt, C. Steenbergen, J. W. Harmon and S. Gerecht, *Proceedings of the National Academy of Sciences*, 2011, 108, 20976-20981.
111. X. Li, S. Chen, B. Zhang, M. Li, K. Diao, Z. Zhang, J. Li, Y. Xu, X. Wang and H. Chen, *International journal of pharmaceutics*, 2012, 437, 110-119.
112. I. Gibas and H. Janik, 2010.
113. P. A. Puolakkainen, D. R. Twardzik, J. E. Ranchalis, S. C. Pankey, M. J. Reed and W. R. Gombotz, *Journal of Surgical Research*, 1995, 58, 321-329.
114. A. J. DeFail, H. D. Edington, S. Matthews, W. C. C. Lee and K. G. Marra, *Journal of Biomedical Materials Research Part A*, 2006, 79, 954-962.
115. M. Kitamura, K. Nakashima, Y. Kowashi, T. Fujii, H. Shimauchi, T. Sasano, T. Furuuchi, M. Fukuda, T. Noguchi and T. Shibutani, *PloS one*, 2008, 3, e2611.
116. K. Hori, C. Sotozono, J. Hamuro, K. Yamasaki, Y. Kimura, M. Ozeki, Y. Tabata and S. Kinoshita, *Journal of controlled release*, 2007, 118, 169-176.
117. A. Zieris, K. Chwalek, S. Prokoph, K. Levental, P. Welzel, U. Freudenberg and C. Werner, *Journal of Controlled Release*, 2011, 156, 28-36.
118. C. Gong, Q. Wu, Y. Wang, D. Zhang, F. Luo, X. Zhao, Y. Wei and Z. Qian, *Biomaterials*, 2013, 34, 6377-6387.
119. I. Banerjee, D. Mishra, T. Das and T. K. Maiti, *Journal of biomaterials science, polymer Edition*, 2012, 23, 111-132.
120. J. Su, J. Li, J. Liang, K. Zhang and J. Li, *Life*, 2021, 11, 1016.
121. D. Wong and J. Parasrampurua, in *Analytical profiles of drug substances and excipients*, Elsevier, 1996, vol. 24, pp. 397-441.
122. J. I. D. Agudelo, M. R. Ramirez, E. R. Henquin and I. Rintoul, *Journal of Materials Chemistry B*, 2019, 7, 4049-4054.
123. X. Liang, H. Ding, Q. Wang, M. Wang, B. Yin and G. Sun, *New Journal of Chemistry*, 2021, 45, 861-871.
124. S. R. Stauffer and N. A. Peppast, *Polymer*, 1992, 33, 3932-3936.
125. N. A. Peppas and J. E. Scott, *Journal of controlled release*, 1992, 18, 95-100.
126. H. Shagholani, S. M. Ghoreishi and R. Rahmatolahzadeh, *BioNanoScience*, 2019, 9, 883-892.
127. J. Maitra and V. K. Shukla, *Am. J. Polym. Sci*, 2014, 4, 25-31.
128. G. S. A. Suleiman, X. Zeng, R. Chakma, I. Y. Wakai and Y. Feng, *Polymers for Advanced Technologies*, 2024, 35, e6327.
129. S. Moulay, *Polymer-Plastics Technology and Engineering*, 2015, 54, 1289-1319.
130. T. Shui, M. Pan, A. Li, H. Fan, J. Wu, Q. Liu and H. Zeng, *Chemistry of Materials*, 2022, 34, 8613-8628.
131. v. H. Deuel and H. Neukom, *Die Makromolekulare Chemie: Macromolecular Chemistry and Physics*, 1949, 3, 13-30.

132. A. Ali, S. P. Nagumantri, T. Rakshit and S. Pal, *Macromolecular Chemistry and Physics*, 2021, 222, 2100121.
133. S. Kitano, K. Kataoka, Y. Koyama, T. Okano and Y. Sakurai, *Die Makromolekulare Chemie, Rapid Communications*, 1991, 12, 227-233.
134. A. Ivanov, H. Larsson, I. Y. Galaev and B. Mattiasson, *Polymer*, 2004, 45, 2495-2505.
135. E. Pezron, L. Leibler, A. Ricard, F. Lafuma and R. Audebert, *Macromolecules*, 1989, 22, 1169-1174.
136. E. Pezron, A. Ricard, F. Lafuma and R. Audebert, *Macromolecules*, 1988, 21, 1121-1125.
137. S. Kesavan and R. K. Prud'Homme, *Macromolecules*, 1992, 25, 2026-2032.
138. D. Power, A. Rodd, L. Paterson and D. Boger, *Journal of Rheology*, 1998, 42, 1021-1037.
139. S. W. Sinton, *Macromolecules*, 1987, 20, 2430-2441.
140. A. Ali, S. Nouseen, S. Saroj, M. Shegane, P. Majumder, A. Puri, T. Rakshit, D. Manna and S. Pal, *Journal of Materials Chemistry B*, 2022, 10, 7591-7599.
141. M. C. Roberts, M. C. Hanson, A. P. Massey, E. A. Karren and P. F. Kiser, *Advanced Materials*, 2007, 19, 2503-2507.
142. M. C. Roberts, A. Mahalingam, M. C. Hanson and P. F. Kiser, *Macromolecules*, 2008, 41, 8832-8840.
143. J. I. Jay, S. Shukair, K. Langheinrich, M. C. Hanson, G. C. Cianci, T. J. Johnson, M. R. Clark, T. J. Hope and P. F. Kiser, *Advanced functional materials*, 2009, 19, 2969-2977.
144. A. Mahalingam, J. I. Jay, K. Langheinrich, S. Shukair, M. D. McRaven, L. C. Rohan, B. C. Herold, T. J. Hope and P. F. Kiser, *Biomaterials*, 2011, 32, 8343-8355.
145. J. I. Jay, K. Langheinrich, M. C. Hanson, A. Mahalingam and P. F. Kiser, *Soft Matter*, 2011, 7, 5826-5835.
146. L. He, D. E. Fullenkamp, J. G. Rivera and P. B. Messersmith, *Chemical Communications*, 2011, 47, 7497-7499.
147. Y. Yu, L. Zhang, B. Hu, Z. Wang, Q. Gu, W. Wang, C. Zhu and S. Wang, *Carbohydrate Polymers*, 2024, 339, 122262.
148. D. J. Murphy, M. G. Sankalia, R. G. Loughlin, R. F. Donnelly, M. G. Jenkins and P. A. McCarron, *International journal of pharmaceuticals*, 2012, 423, 326-334.
149. Q. Zhang, N. R. Ko and J. K. Oh, *RSC advances*, 2012, 2, 8079-8086.
150. J. G. Lees, A. J. Miles, F. Wien and B. A. Wallace, *Bioinformatics*, 2006, 22, 1955-1962.
151. A. H. Zisch, M. P. Lutolf, M. Ehrbar, G. P. Raeber, S. C. Rizzi, N. Davies, H. Schmökel, D. Bezuidenhout, V. Djonov and P. Zilla, *The FASEB journal*, 2003, 17, 2260-2262.
152. M. A. Nunes, P. M. Gois, M. E. Rosa, S. Martins, P. C. Fernandes and M. H. Ribeiro, *Tetrahedron*, 2016, 72, 7293-7305.
153. E. L. Daniels, J. R. Runge, M. Oshinowo, H. S. Leese and A. Buchard, *ACS Applied Energy Materials*, 2023, 6, 2924-2935.
154. R. Ghosh, S. Roy and B. Bagchi, *arXiv preprint arXiv:1307.2737*, 2013.
155. M. Mukai, W. Ma, K. Ideta and A. Takahara, *Polymer*, 2019, 178, 121581.
156. D. G. Hall, *Chemical Society Reviews*, 2019, 48, 3475-3496.
157. M. A. Bridges, K. M. McErlane, E. Kwong, S. Katz and D. A. Applegarth, *Clinica chimica acta*, 1986, 157, 73-79.
158. G. M. Funk, C. Hunt, D. Epps and P. Brown, *Journal of lipid research*, 1988, 27, 792-795.
159. M. Li, S. Jiang, J. Simon, D. Paßlick, M.-L. Frey, M. Wagner, V. Mailänder, D. Crespy and K. Landfester, *Nano Letters*, 2021, 21, 1591-1598.

160. A. Pritzlaff, G. Ferré, E. Mulry, L. Lin, N. Gopal Pour, D. A. Savin, M. E. Harris and M. T. Eddy, *Angewandte Chemie International Edition*, 2022, 61, e202203784.
161. G. Bashiri, M. S. Padilla, K. L. Swingle, S. J. Shepherd, M. J. Mitchell and K. Wang, *Lab on a Chip*, 2023, 23, 1432-1466.